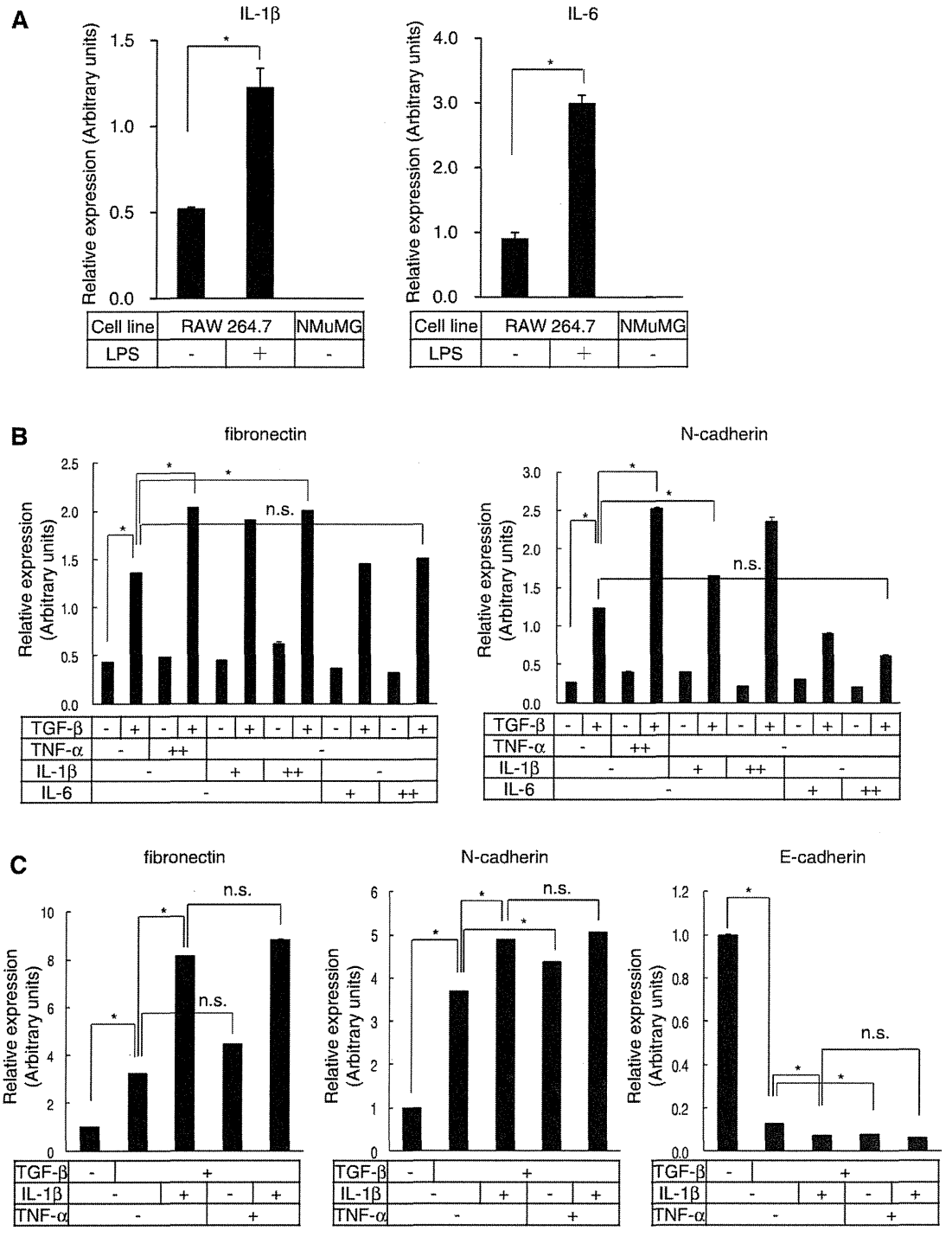

Fig. 6 Effect of IL-1β and IL-6 on TGF-β-induced expression of EMT markers. (A) qRT–PCR analysis of expression of IL-1β and IL-6 in RAW 264.7 cells treated with 0.1 μg/ml LPS was performed. NMuMG cells served as a negative control. The samples used in Fig. 3A were used for the analysis. (B) Effect of IL-1β and IL-6 on the expression of fibronectin and N-cadherin was determined using qRT–PCR in A549 cells. Cells were treated with 5 ng/ml TGF-β, 20 ng/ml TNF-α, 1 ng/ml (+) or 20 ng/ml (++) of IL-1β and IL-6 for 24 h. (C) A549 cells were treated with 1 ng/ml IL-1β, 20 ng/ml TNF-α, or both in the presence of TGF-β. $*P<0.05$; Error bars, SDs; n.s., not significant.

proteoglycan, is also secreted from cancer cells and is reported to activate macrophages and induce cancer cell invasion and metastasis (*42*). Whether A549 cells affect RAW 264.7 cells to secrete the factors that regulate EMT of A549 cells requires further investigation.

The mechanisms underlying the enhancement of TGF-β-induced EMT by TNF-α in A549 cells are poorly understood. Liu reported upregulation of TGFBR1 by inflammatory cytokines (*35*). However, upregulation of TGFBR1 mRNA was primarily induced by TGF-β in our analysis, and the effect of

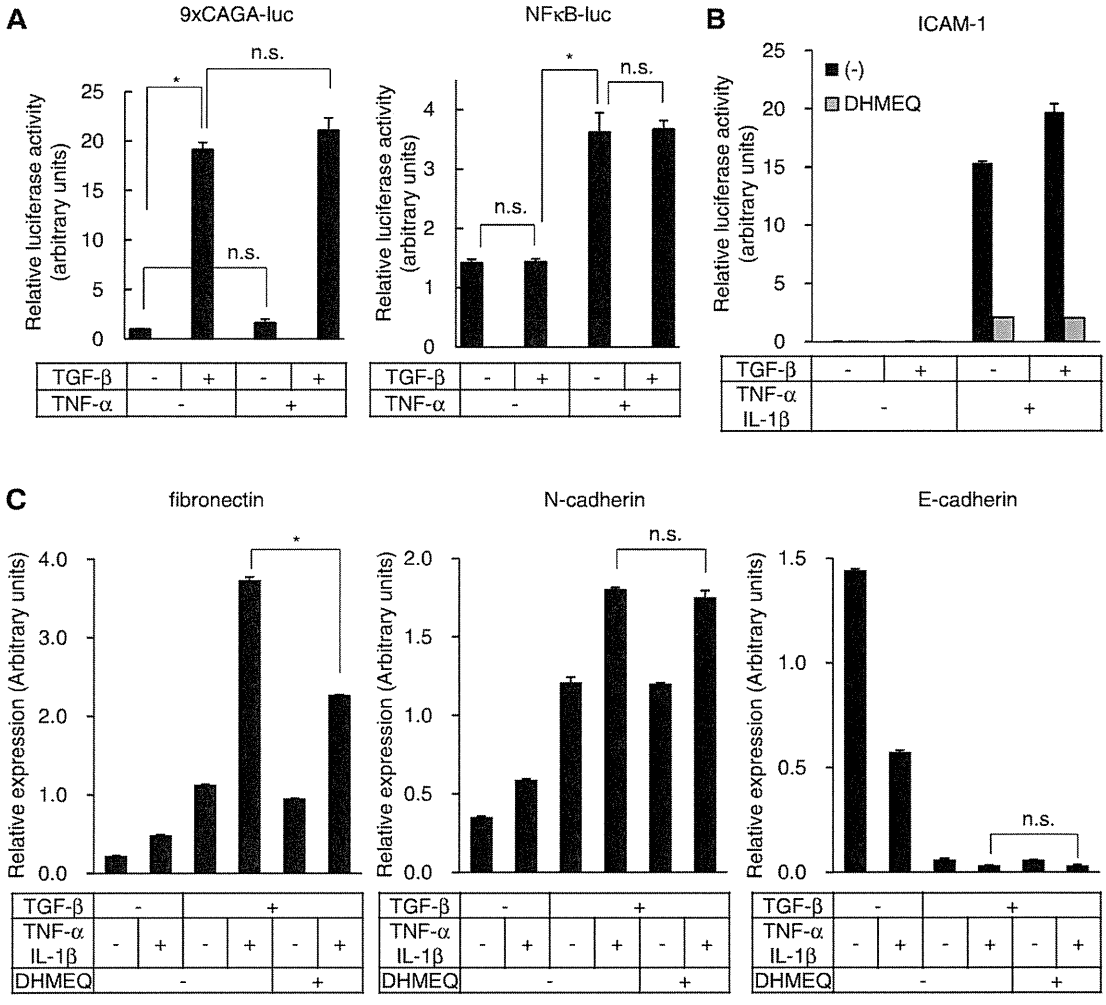

Fig. 7 Effect of DHMEQ on the enhancement of EMT marker expression by TNF-α and IL-1β. (A) A 9xCAGA-luc luciferase construct consisting of tandemly repeated Smad binding elements and NF-κB-luc luciferase reporter construct were transfected in A549 cells and stimulated with 5 ng/ml of TGF-β and 20 ng/ml of TNF-α for 24 h (9xCAGA-luc) or 6 h (NFκB-luc). (B) Inhibition of TNF-α and IL-1β-induced ICAM-1 expression by DHMEQ. A549 cells were pre-treated with 10 μg/ml of DHMEQ or DMSO as a control for 3.5 h and stimulated by TNF-α and IL-1β for 4 h. ICAM-1 expression was measured by qRT–PCR. (C) A549 cells were treated as in (B), and stimulated with TGF-β, TNF-α and IL-1β for 24 h. Expression of EMT markers was analysed by qRT–PCR. $*P<0.05$; Error bars, SDs; n.s., not significant.

TNF-α was observed only in the presence of TGF-β. Nevertheless, TGF-β-induced phosphorylation of Smad2, and Smad-induced 9xCAGA luciferase reporter activity did not change following the addition of TNF-α. We also observed that TGF-β does not enhance TNF-α-induced transcriptional activity of NFκB-luc, and that enhanced expression of target genes by TNF-α was selective to fibronectin and N-cadherin. Although many reports have revealed crosstalk between TNF-α and TGF-β signalling pathways in a variety of cells (*43*, *44*), the present analyses suggest that the cooperation of these cytokines appears to be exerted at the transcription level of each target gene depending on the context of their *cis*-regulatory elements, indicating differences in the transcriptional responses of target genes (*34*, *45*, *46*). Thus, neutralizing antibody against TNF-α inhibited the expression of both fibronectin and N-cadherin. In contrast, only the expression of fibronectin was inhibited by DHMEQ and U0126, whereas that of N-cadherin was inhibited by SB203580. Combinatorial effects of the several inhibitors on EMT phenotypes including expression of fibronectin and N-cadherin in the context of co-stimulation by TGF-β and inflammatory cytokines need to be evaluated in the future analyses.

The importance of EMT in cancer pathophysiology is not limited to cancer cell invasion and metastasis. Asiedu et al. reported generation of breast cancer stem cells by TNF-α and TGF-β (*47*). Based on our analyses suggesting the importance of TNF-α on TGF-β-induced EMT in A549 cells at a level of endogenous secretion from RAW 264.7 cells, complex mechanisms of enhancement by TNF-α require further examination to develop methods for controlling tumour cell invasion and cancer stem cells.

Supplementary Data

Supplementary Data are available at *JB* online.

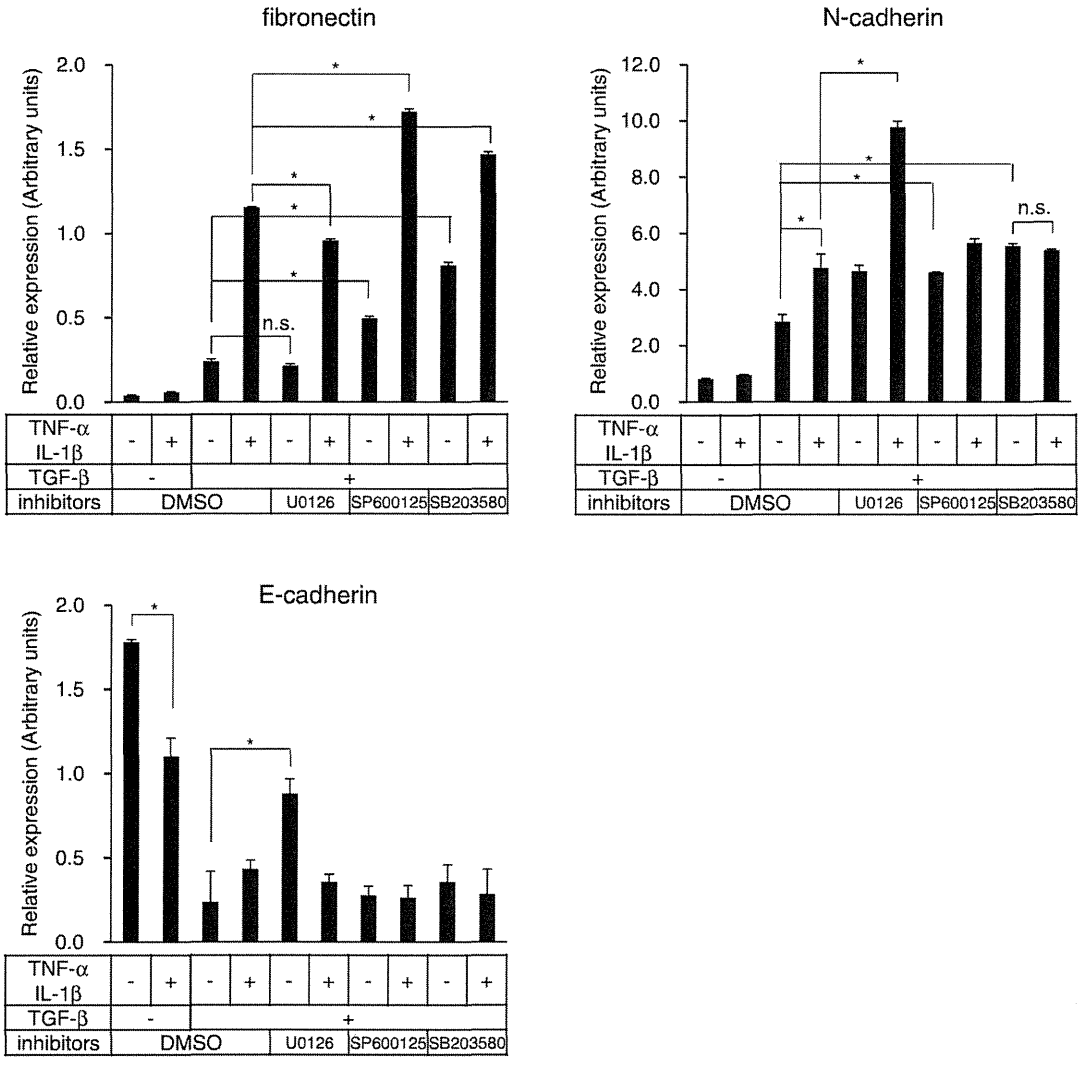

Fig. 8 Effect of kinase inhibitors on enhancement of TGF-β-induced EMT by TNF-α and IL-1β. A549 cells were pre-treated with either 10 μM U0126 (MEK inhibitor), 1 μM SP600125 (JNK inhibitor) or 1 μM SB203580 (p38 inhibitor) for 3.5 h. Cells were then stimulated with 5 ng/ml TGF-β, 20 ng/ml TNF-α and 1 ng/ml IL-1β for 24 h. Expression of EMT markers was determined by qRT–PCR after 24-h stimulation and normalized by GAPDH. $*P<0.05$; Error bars, SDs; n.s., not significant.

Acknowledgements

The authors thank Keiko Yuki and Yasuyuki Morishita for technical assistance.

Funding

KAKENHI [Grants-in-aid for Scientific Research on Innovative Areas (Integrative Research on Cancer Microenvironment Network grant 22112002 to K.M.) and for young scientists (B) (22790750 to D.K.)] from the Ministry of Education, Culture, Sports, Science, and Technology of Japan (MEXT); the Global Center of Excellence Program (Integrative Life Science Based on the Study of Biosignaling Mechanisms) from the Japan Society for the Promotion of Science.

Conflict of interest

None declared.

References

1. Bierie, B. and Moses, H.L. (2006) Tumour microenvironment: TGF-β: the molecular Jekyll and Hyde of cancer. *Nat. Rev. Cancer* **6**, 506–520
2. Ikushima, H. and Miyazono, K. (2010) TGF-β signalling: a complex web in cancer progression. *Nat. Rev. Cancer* **10**, 415–424
3. Yoshimura, A., Wakabayashi, Y., and Mori, T. (2010) Cellular and molecular basis for the regulation of inflammation by TGF-β. *J. Biochem.* **147**, 781–792
4. Derynck, R., Akhurst, R.J., and Balmain, A. (2001) TGF-β signaling in tumor suppression and cancer progression. *Nat. Genet.* **29**, 117–129
5. Sabe, H. (2011) Cancer early dissemination: cancerous epithelial-mesenchymal transdifferentiation and transforming growth factor-β signalling. *J. Biochem.* **149**, 633–639
6. Miyazono, K. (2009) Transforming growth factor-β signaling in epithelial-mesenchymal transition and progression of cancer. *Proc. Jpn. Acad. Ser. B Phys. Biol. Sci.* **85**, 314–323
7. Meulmeester, E. and ten Dijke, P. (2011) The dynamic roles of TGF-β in cancer. *J. Pathol.* **223**, 205–218
8. Heldin, C.H., Miyazono, K., and ten Dijke, P. (1997) TGF-β signalling from cell membrane to nucleus through SMAD proteins. *Nature* **390**, 465–471

9. Miyazono, K., Kamiya, Y., and Morikawa, M. (2010) Bone morphogenetic protein receptors and signal transduction. *J. Biochem.* **147**, 35–51
10. Thuault, S., Valcourt, U., Petersen, M., Manfioletti, G., Heldin, C.H., and Moustakas, A. (2006) Transforming growth factor-β employs HMGA2 to elicit epithelial-mesenchymal transition. *J. Cell Biol.* **174**, 175–183
11. Shirakihara, T., Saitoh, M., and Miyazono, K. (2007) Differential regulation of epithelial and mesenchymal markers by δEF1 proteins in epithelial mesenchymal transition induced by TGF-β. *Mol. Biol. Cell* **18**, 3533–3544
12. Kondo, M., Cubillo, E., Tobiume, K., Shirakihara, T., Fukuda, N., Suzuki, H., Shimizu, K., Takehara, K., Cano, A., Saitoh, M., and Miyazono, K. (2004) A role for Id in the regulation of TGF-β-induced epithelial-mesenchymal transdifferentiation. *Cell Death Differ.* **11**, 1092–1101
13. Vincent, T., Neve, E.P., Johnson, J.R., Kukalev, A., Rojo, F., Albanell, J., Pietras, K., Virtanen, I., Philipson, L., Leopold, P.L., Crystal, R.G., de Herreros, A.G., Moustakas, A., Pettersson, R.F., and Fuxe, J. (2009) A SNAIL1-SMAD3/4 transcriptional repressor complex promotes TGF-β mediated epithelial-mesenchymal transition. *Nat. Cell Biol.* **11**, 943–950
14. Thuault, S., Tan, E.J., Peinado, H., Cano, A., Heldin, C.H., and Moustakas, A. (2008) HMGA2 and Smads co-regulate SNAIL1 expression during induction of epithelial-to-mesenchymal transition. *J. Biol. Chem.* **283**, 33437–33446
15. Morita, T., Mayanagi, T., and Sobue, K. (2007) Dual roles of myocardin-related transcription factors in epithelial mesenchymal transition via slug induction and actin remodeling. *J. Cell Biol.* **179**, 1027–1042
16. Mihira, H., Suzuki, H., Akatsu, Y., Yoshimatsu, Y., Igarashi, T., Miyazono, K., and Watabe, T. (2011) TGF-β-induced mesenchymal transition of MS-1 endothelial cells requires Smad-dependent cooperative activation of Rho signals and MRTF-A. *J. Biochem.*, doi:10.1093/jb/mvr121
17. Saito, R.A., Watabe, T., Horiguchi, K., Kohyama, T., Saitoh, M., Nagase, T., and Miyazono, K. (2009) Thyroid transcription factor-1 inhibits transforming growth factor-β-mediated epithelial-to-mesenchymal transition in lung adenocarcinoma cells. *Cancer Res.* **69**, 2783–2791
18. Moustakas, A. and Heldin, C.H. (2007) Signaling networks guiding epithelial-mesenchymal transitions during embryogenesis and cancer progression. *Cancer Sci.* **98**, 1512–1520
19. Shirakihara, T., Horiguchi, K., Miyazawa, K., Ehata, S., Shibata, T., Morita, I., Miyazono, K., and Saitoh, M. (2011) TGF-β regulates isoform switching of FGF receptors and epithelial-mesenchymal transition. *EMBO J.* **30**, 783–795
20. Maier, H.J., Schmidt-Strassburger, U., Huber, M.A., Wiedemann, E.M., Beug, H., and Wirth, T. (2010) NF-κB promotes epithelial-mesenchymal transition, migration and invasion of pancreatic carcinoma cells. *Cancer Lett.* **295**, 214–228
21. Borthwick, L.A., McIlroy, E.I., Gorowiec, M.R., Brodlie, M., Johnson, G.E., Ward, C., Lordan, J.L., Corris, P.A., Kirby, J.A., and Fisher, A.J. (2010) Inflammation and epithelial to mesenchymal transition in lung transplant recipients: role in dysregulated epithelial wound repair. *Am. J. Transplant.* **10**, 498–509
22. Kasai, H., Allen, J.T., Mason, R.M., Kamimura, T., and Zhang, Z. (2005) TGF-β1 induces human alveolar epithelial to mesenchymal cell transition (EMT). *Respir. Res.* **6**, 56
23. Umezawa, K., Ariga, A., and Matsumoto, N. (2000) Naturally occurring and synthetic inhibitors of NF-κB functions. *Anticancer Drug Des.* **15**, 239–244
24. Matsumoto, N., Ariga, A., To-e, S., Nakamura, H., Agata, N., Hirano, S., Inoue, J., and Umezawa, K. (2000) Synthesis of NF-κB activation inhibitors derived from epoxyquinomicin C. *Bioorg. Med. Chem. Lett.* **10**, 865–869
25. Nagano, Y., Koinuma, D., Miyazawa, K., and Miyazono, K. (2010) Context-dependent regulation of the expression of c-Ski protein by Arkadia in human cancer cells. *J. Biochem.* **147**, 545–554
26. Horiguchi, K., Shirakihara, T., Nakano, A., Imamura, T., Miyazono, K., and Saitoh, M. (2009) Role of Ras signaling in the induction of snail by transforming growth factor-β. *J. Biol. Chem.* **284**, 245–253
27. Nagata, M., Nagata, S., Yuki, K., Isogaya, K., Saitoh, M., Miyazono, K., and Miyazawa, K. (2010) Identification of a phosphorylation site in c-Ski as serine 515. *J. Biochem.* **148**, 423–427
28. Mizutani, A., Saitoh, M., Imamura, T., Miyazawa, K., and Miyazono, K. (2010) Arkadia complexes with clathrin adaptor AP2 and regulates EGF signalling. *J. Biochem.* **148**, 733–741
29. Soll, D.R., Voss, E., Varnum-Finney, B., and Wessels, D. (1988) "Dynamic Morphology System": a method for quantitating changes in shape, pseudopod formation, and motion in normal and mutant amoebae of Dictyostelium discoideum. *J. Cell. Biochem.* **37**, 177–192
30. Katsuno, Y., Hanyu, A., Kanda, H., Ishikawa, Y., Akiyama, F., Iwase, T., Ogata, E., Ehata, S., Miyazono, K., and Imamura, T. (2008) Bone morphogenetic protein signaling enhances invasion and bone metastasis of breast cancer cells through Smad pathway. *Oncogene* **27**, 6322–6333
31. Nakano, A., Koinuma, D., Miyazawa, K., Uchida, T., Saitoh, M., Kawabata, M., Hanai, J., Akiyama, H., Abe, M., Miyazono, K., Matsumoto, T., and Imamura, T. (2009) Pin1 down-regulates transforming growth factor-β (TGF-β) signaling by inducing degradation of Smad proteins. *J. Biol. Chem.* **284**, 6109–6115
32. Dennler, S., Itoh, S., Vivien, D., ten Dijke, P., Huet, S., and Gauthier, J.M. (1998) Direct binding of Smad3 and Smad4 to critical TGF-β-inducible elements in the promoter of human plasminogen activator inhibitor-type I gene. *EMBO J.* **17**, 3091–3100
33. Lernbecher, T., Muller, U., and Wirth, T. (1993) Distinct NF-κ B/Rel transcription factors are responsible for tissue-specific and inducible gene activation. *Nature* **365**, 767–770
34. Mizutani, A., Koinuma, D., Tsutsumi, S., Kamimura, N., Morikawa, M., Suzuki, H.I., Imamura, T., Miyazono, K., and Aburatani, H. (2011) Cell-type specific target selection by combinatorial binding of Smad2/3 and hepatocyte nuclear factor 4-α in HepG2 cells. *J. Biol. Chem.* **286**, 29848–29860
35. Liu, X. (2008) Inflammatory cytokines augments TGF-β1-induced epithelial-mesenchymal transition in A549 cells by up-regulating TβR-I. *Cell Motil. Cytoskeleton* **65**, 935–944
36. Kim, J.H., Jang, Y.S., Eom, K.S., Hwang, Y.I., Kang, H.R., Jang, S.H., Kim, C.H., Park, Y.B., Lee, M.G., Hyun, I.G., Jung, K.S., and Kim, D.G. (2007)

Transforming growth factor β1 induces epithelial-to-mesenchymal transition of A549 cells. *J. Korean Med. Sci.* **22**, 898–904

37. Yamauchi, Y., Kohyama, T., Takizawa, H., Kamitani, S., Desaki, M., Takami, K., Kawasaki, S., Kato, J., and Nagase, T. (2010) Tumor necrosis factor-α enhances both epithelial-mesenchymal transition and cell contraction induced in A549 human alveolar epithelial cells by transforming growth factor-β1. *Exp. Lung Res.* **36**, 12–24
38. Camara, J. and Jarai, G. (2010) Epithelial-mesenchymal transition in primary human bronchial epithelial cells is Smad-dependent and enhanced by fibronectin and TNF-α. *Fibrogenesis Tissue Repair* **3**, 2
39. Kamitani, S., Yamauchi, Y., Kawasaki, S., Takami, K., Takizawa, H., Nagase, T., and Kohyama, T. (2011) Simultaneous stimulation with TGF-β1 and TNF-α induces epithelial mesenchymal transition in bronchial epithelial cells. *Int. Arch. Allergy Immunol.* **155**, 119–128
40. Schulz, C., Farkas, L., Wolf, K., Kratzel, K., Eissner, G., and Pfeifer, M. (2002) Differences in LPS-induced activation of bronchial epithelial cells (BEAS-2B) and type II-like pneumocytes (A-549). *Scand. J. Immunol.* **56**, 294–302
41. Tsutsumi-Ishii, Y. and Nagaoka, I. (2003) Modulation of human β-defensin-2 transcription in pulmonary epithelial cells by lipopolysaccharide-stimulated mononuclear phagocytes via proinflammatory cytokine production. *J. Immunol.* **170**, 4226–4236
42. Kim, S., Takahashi, H., Lin, W.W., Descargues, P., Grivennikov, S., Kim, Y., Luo, J.L., and Karin, M. (2009) Carcinoma-produced factors activate myeloid cells through TLR2 to stimulate metastasis. *Nature* **457**, 102–106
43. Takahashi, E., Nagano, O., Ishimoto, T., Yae, T., Suzuki, Y., Shinoda, T., Nakamura, S., Niwa, S., Ikeda, S., Koga, H., Tanihara, H., and Saya, H. (2010) Tumor necrosis factor-α regulates transforming growth factor-β-dependent epithelial-mesenchymal transition by promoting hyaluronan-CD44-moesin interaction. *J. Biol. Chem.* **285**, 4060–4073
44. Bitzer, M., von Gersdorff, G., Liang, D., Dominguez-Rosales, A., Beg, A.A., Rojkind, M., and Bottinger, E.P. (2000) A mechanism of suppression of TGF-β/SMAD signaling by NF-κ B/RelA. *Genes Dev.* **14**, 187–197
45. Gomis, R.R., Alarcon, C., He, W., Wang, Q., Seoane, J., Lash, A., and Massague, J. (2006) A FoxO-Smad synexpression group in human keratinocytes. *Proc. Natl. Acad. Sci. USA* **103**, 12747–12752
46. Koinuma, D., Tsutsumi, S., Kamimura, N., Taniguchi, H., Miyazawa, K., Sunamura, M., Imamura, T., Miyazono, K., and Aburatani, H. (2009) Chromatin immunoprecipitation on microarray analysis of Smad2/3 binding sites reveals roles of ETS1 and TFAP2A in transforming growth factor β signaling. *Mol. Cell. Biol.* **29**, 172–186
47. Asiedu, M.K., Ingle, J.N., Behrens, M.D., Radisky, D.C., and Knutson, K.L. (2011) TGF-β/TNF-α-mediated epithelial-mesenchymal transition generates breast cancer stem cells with a claudin-low phenotype. *Cancer Res.* **71**, 4707–4719

JDA Japanese Dermatological Association
THE JOURNAL OF DERMATOLOGY
doi: 10.1111/j.1346-8138.2011.01396.x
Journal of Dermatology 2012; **39**: 366–374

ORIGINAL ARTICLE

Targeted overexpression of Angptl6/angiopoietin-related growth factor in the skin promotes angiogenesis and lymphatic vessel enlargement in response to ultraviolet B

Hidenori OKAZAKI,[1] Satoshi HIRAKAWA,[2] Masachika SHUDOU,[3] Yoshiki NAKAOKA,[1] Yuji SHIRAKATA,[1] Keishi MIYATA,[4,5] Yuichi OIKE,[4] Koji HASHIMOTO,[1] Koji SAYAMA[1]

[1]*Department of Dermatology, Ehime University Graduate School of Medicine, Ehime,* [2]*Department of Dermatology, Hamamatsu University School of Medicine, Shizuoka,* [3]*Department of Bioscience, Ehime University, Ehime,* [4]*Departments of Molecular Genetics, and* [5]*Immunology, Allergy and Vascular Medicine, Graduate School of Medical Sciences, Kumamoto University, Kumamoto, Japan*

ABSTRACT

Angiogenesis is required for physiological tissue repair processes, such as cutaneous wound healing. However, recent studies indicate that endogenous angiogenic factors may enhance photo-induced skin alterations in response to experimental ultraviolet (UV)-B exposure. Angiopoietin-related growth factor (AGF), also known as angiopoietin-like protein 6 (Angptl6), is known to promote new blood vessel formation and vascular hyperpermeability. Importantly, epidermal overexpression of Angptl6/AGF in mice promotes wound healing in the skin. However, it remains unclear whether overexpression of Angptl6/AGF facilitates tissue repair processes in response to UV-B irradiation. To test this hypothesis, we subjected *Angptl6/AGF* transgenic mice to acute or chronic UV-B exposure. Surprisingly, transgenic mice showed enhanced photosensitivity to subthreshold doses of UV-B that did not induce skin alterations in wild-type littermates. Marked enlargement of blood vessels was observed after a single exposure to UV-B in *Angptl6/AGF* transgenic mice, although no epidermal changes were observed. Chronic UV-B exposure over 14 weeks promoted cutaneous skin damage in *Angptl6/AGF* transgenic mice, whereas wild-type mice showed little or no macroscopic skin alteration. In addition to pronounced angiogenesis and epidermal hyperplasia, marked enlargement of dermal lymphatic vessels was observed in UV-B-exposed *Angptl6/AGF* transgenic mice. Electron microscopy analysis further revealed that the number and size of collagen bundles in the dermis was markedly reduced after chronic UV-B exposure in *Angptl6/AGF* transgenic mice. Taken together, these results indicate that ectopic expression of Angptl6/AGF in mice likely promotes UV-B-induced skin alterations, and that angiogenesis could be a therapeutic target in prevention of skin photo-aging.

Key words: collagen, photoaging, photosensitivity, transgenic mice, vascular endothelial growth factor.

INTRODUCTION

Angiogenesis – the formation of new blood vessels from pre-existing ones – is induced in physiological tissue repair and in pathological conditions such as cutaneous inflammation and/or tumor progression.[1,2] Ultraviolet (UV)-B induces acute and chronic skin alterations. Acute exposure of human or mouse skin to UV-B promotes erythema and/or blisters because of marked increases in vascular permeability. UV-B-induced skin damage is characterized by epidermal hyperplasia, degradation of matrix proteins and dermal elastosis.[3] Previous studies have shown that pronounced angiogenesis is induced by acute UV-B irradiation of human and mouse skin.[4,5] In fact, UV-B irradiation upregulates potent angiogenic factors in the skin, including vascular endothelial growth factor (VEGF)-A, basic fibroblast growth factor and interleukin-8.[6–8] Overexpression of VEGF-A in the epidermis has also been shown to induce enhanced photosensitivity in the skin in response to a single UV-B exposure.[9] In contrast, systemic blockade of endogenous VEGF-A signaling significantly reduces photosensitivity and antagonizes enlargement of blood vessels in the skin, indicating that the primary angiogenic response may be the crucial event that facilitates acute photo-induced skin reactions. Importantly, chronic UV-B exposure caused prominent wrinkle formation in VEGF-A transgenic mice by promoting significant new blood vessel formation in the skin, leading to the idea that endogenous angiogenic factors such as VEGF-A function to promote photo-induced skin damage. Currently, it is unclear whether ectopic expression of angiogenic growth factors contributes to cutaneous tissue repair processes in response to UV-B exposure.

Angiopoietin-related growth factor (AGF), also known as Angptl6, is a member of the family of angiopoietin-like proteins, which play crucial roles in murine vascular development and/or physiological

Correspondence: Satoshi Hirakawa, M.D., Ph.D., Department of Dermatology, Hamamatsu University School of Medicine, 1-20-1 Handayama, Higashi-ku, Hamamatsu-shi, Shizuoka 431-3192, Japan. Email: hirakawa@hama-med.ac.jp
Received 17 July 2011; accepted 25 July 2011.

metabolism.[10,11] Like all angiopoietins, Angptl6/AGF possesses an N-terminal coiled-coil domain and a C-terminal fibrinogen-like domain.[12] Most angiopoietins are known to bind Tie1 and/or Tie2 receptors, whereas Angptl6/AGF remains an orphan ligand. Targeted disruption of *Angptl6/AGF* in mice leads to obesity and insulin resistance, reflecting clinical features reminiscent of human metabolic syndrome.[11] Meanwhile, targeted overexpression of Angptl6/AGF in mouse skin promotes angiogenesis and epidermal hyperplasia, indicating that Angptl6/AGF mediates pleiotropic effects towards several cell lineages, including epidermal keratinocytes.[10,13] Of particular interest, Angptl6/AGF transgenic mice in the skin show markedly enhanced cutaneous wound healing during the tissue repair process compared to wild-type mice.[13] Importantly, little or no Angptl6/AGF is expressed endogenously in mouse skin, indicating that Angptl6/AGF has a potent tissue repair function separate from its role as an angiogenic factor in the skin.

Recent studies indicate that lymphatic vessels play a crucial role in mediating UV-B-induced cutaneous changes.[14] UV-B exposure induces marked enlargement of lymphatic vessels in mouse skin. Sufficient lymphatic flow is required to suppress dermal edema and inflammation in response to a single UV-B exposure. Importantly, activation of VEGF-C/vascular endothelial growth factor receptor-3, one of the major pathways promoting lymphatic vessel growth and function,[15] has been shown to attenuate UV-B-induced edema formation and skin inflammation.[16] Furthermore, lymphatic vessels show enhanced leakiness in UV-B-irradiated skin, leading to reduced lymphatic drainage and impaired function.[14] Moreover, among Angptl family members, targeted Angptl2 overexpression in the skin has been recently shown to promote enlargement of dermal lymphatic as well as blood vessels.[17] Currently, it is unclear whether Angptl6/AGF alters the growth of lymphatic vessels in experimental mouse models of UV-B exposure.

Here, to test the hypothesis whether AGF facilitates cutaneous tissue repair processes in response to UV-B irradiation, we subjected *Angptl6/AGF* transgenic mice to either acute or chronic UV-B exposure. We report that overexpression of Angptl6/AGF in mouse skin enhances photosensitivity to acute UV-B exposure by promoting enlargement of dermal blood vessels but does not induce epidermal hyperplasia in response to a minimal erythema dose of UV-B. By contrast, chronic UV-B exposure, at a dose that did not induce detectable skin changes in wild-type mice, induced pronounced angiogenesis and enlargement of lymphatic vessels, leading to wrinkle development in *Angptl6/AGF* transgenic mice. Together, these results indicate that targeted overexpression of Angptl6/AGF in mouse skin may prevent photo-induced cutaneous damage from a single exposure of UV-B, but long-term AGF induction could mediate UV-B-induced skin alterations such as photo-induced skin aging.

METHODS

UV-B irradiation regime

Ten-week-old male FVB/N or BALB/c wild-type mice, or keratin 14 promoter-driven *Angptl6/AGF* transgenic mice were exposed to graded doses of four equally charged fluorescent lamps (ULTRAVIOLET-B TL 20W/12RS; Philips, Amsterdam, Netherlands). The minimal erythema dose (MED) was determined by irradiation of square areas on back skin with seven different doses of UV-B, ranging 5.0×10^{-2} to 4.0×10^{-1} J/cm^2 (n = 5/group). An additional skin area was sham-irradiated. Erythema formation was evaluated 48 h after irradiation. Ten-week-old male BALB/c wild-type mice or transgenic overexpressing Angptl6/AGF in the epidermis under control of the human keratin 14 promoter were exposed to seven different UV-B doses, ranging 3.0×10^{-2} to 9.0×10^{-2} J/cm^2, on the dorsal skin (n = 5/group) to determine MED. In addition, ear skin of AGF transgenic mice and wild-type littermates was exposed to a single dose of UV-B by 9.0×10^{-2} J/cm^2 (n = 5/group). Thereafter, ear thickness was measured daily for up to 8 days. In an additional experiment, 8-week-old male wild-type or AGF transgenic mice were irradiated three times weekly for 14 weeks with a total dose of 8.185 J/cm^2 (n = 10/genotype). Control mice were sham-irradiated. Skin samples were either snap-frozen with O.C.T.-Compound (Sakura Finetek Japan, Tokyo, Japan) in ethanol dry ice or fixed in 4% paraformaldehyde in phosphate-buffered saline. All animal studies were approved by the Ehime University Subcommittee on Research Animal Care.

Real-time reverse transcription polymerase chain reaction (RT–PCR)

Total RNA was isolated from dorsal skin of *Angptl6/AGF* transgenic mice or wild-type littermates (n = 5) and of five non-irradiated control mice using Isogen (Wako, Osaka, Japan). Real-time RT–PCR was performed and analyzed with a 7900 HT Fast Real-Time PCR System (Applied Biosystems, Branchburg, NJ, USA). Primers and probes for β-actin, AGF, VEGF-A, VEGF-C and VEGF-D were purchased from Applied Biosystems. RNA analysis was carried out using a TaqMan RT–PCR Master Mix reagents kit (Applied Biosystems), according to the manufacturer's protocol. Target gene expression in test samples was normalized to corresponding β-actin expression.

Histological analysis and immunofluorescence stains

Immunofluorescence was analyzed on 5-μm frozen sections, as described previously,[18] using a biotinylated rat antimouse CD31 antibody (BD Biosciences Pharmingen, San Diego, CA, USA), a monoclonal rat LYVE-1 antibody (MBL, Nagoya, Japan), and corresponding secondary antibodies labeled with Alexa Fluor 488 or 594 (Molecular Probes, Eugene, OR, USA). Representative sections were prepared from skin of UV-B- or sham-irradiated mice (n = 5/group). Nuclei were counterstained with 4′,6′-diamidino-2-phenylindole dihydrochloride (DAPI; Molecular Probes). Staining was analyzed and digital images were captured using a confocal laser scanning microscope LSM510 (Carl Zeiss, Jena, Germany). Morphometric analyses were performed using IP-LAB software as described previously.[19] In addition, paraffin sections were prepared from skin of the same mice. Routine hematoxylin–eosin or Masson-trichrome staining was performed.

Computer-assisted morphometric vessel analysis

Double immunofluorescence staining using anti-CD31 antibody for blood vessels and anti-LYVE-1 antibody for lymphatic vessels was analyzed using an LSM510 microscope. Representative fields of

each section were examined at ×10 magnification, and the number of vessels/mm^2, average vessel size and relative area occupied by blood or lymphatic vessels were determined in a dermal area within 200 μm of the epidermal–dermal junction. An unpaired Student's *t*-test was used to analyze differences in microvessel density, vascular size and relative vascular area.

Transmission electron microscopy analysis

Skin tissues were fixed in 0.1 mol/L phosphate-buffered 2.5% glutaraldehyde with 0.1% tannic acid (pH 7.4) for 2 h, and postfixed with 1% osmium tetroxide in phosphate buffer for 2 h. Specimens were washed in 0.25 mol/L sucrose solution, dehydrated in a graded ethanol series, and embedded in an Epon resin mixture (*Epon 812 resin*; TAAB Laboratories Equipment, Aldermaston, Berks, England). Ultra-thin sections of 60–80 nm were prepared using an Ultracut S blade (Leica Microsystems, Wetzlar, Germany) and subsequently double-stained with uranyl acetate and lead citrate. Specimens were analyzed at a voltage of 80 kV, and images were captured using a transmission electron microscope, JEM-1230 (JEOL, Tokyo, Japan).

RESULTS

BALB/c and FVB/N wild-type mice show comparable MED

Transgenic mice in which Angptl6/AGF is driven from the keratin 14 promoter (*K14–Angptl6/AGF*) were originally bred on a BALB/c background.[13] However, previous studies of the role of angiogenesis in mediating UV-B-induced skin alterations in transgenic mice have utilized mice on an FVB/N background.[4,9] Therefore, to assess the biological effect of Angptl6/AGF upon photodamaged skin, we first compared the MED of wild-type FVB/N and BALB/c mice using graded UV-B doses. The dorsal skin of FVB/N wild-type mice showed signs of erythema 48 h after irradiation with 7.2×10^{-2} J/cm^2 UV-B or higher doses (n = 6) (Fig. 1a). Similarly, BALB/c wild-type mice developed minimal erythema on back skin at a dose of 7.2×10^{-2} J/cm^2 UV-B (n = 6) (Fig. 1b) in the same timeframe. Therefore, both FVB/N and BALB/c wild-type mice showed comparable erythema formation at the same radiation dose, indicating that BALB/c mice are suitable models to evaluate photosensitivity following UV-B radiation.

Cutaneous photosensitivity is enhanced in *Angptl6/AGF* transgenic mice

To determine whether epidermal Angptl6/AGF overexpression alters cutaneous photosensitivity in the skin, we evaluated MED of *Angptl6/AGF* transgenic mice by exposing them to doses of UV-B ranging 3.0×10^{-2} to 9.0×10^{-2} J/cm^2. The dorsal skin of AGF transgenic mice showed signs of erythema at 4.0×10^{-2} J/cm^2 UV-B and higher (n = 5) (Fig. 1d), whereas in comparably-treated wild-type littermates the MED was defined as 7.2×10^{-2} J/cm^2 UV-B (Fig. 1c). Statistical analysis showed that the MED for *Angptl6/AGF* transgenic mice is significantly lower than that of wild-type mice (Fig. 1e). Overall, these observations suggest that Angptl6/AGF transgenic mice show enhanced cutaneous photosensitivity relative to wild-type mice.

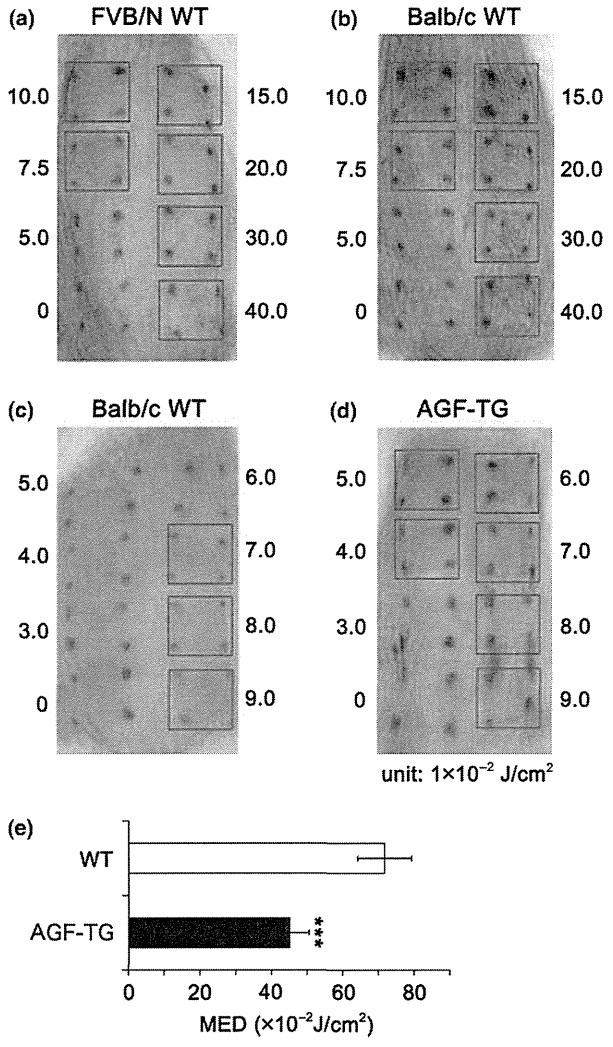

Figure 1. Enhanced photosensitivity of *Angptl6/AGF* transgenic (TG) mice. (a,b) The dorsal skin was exposed to graded doses of ultraviolet (UV)-B ranging 5.0×10^{-2} to 4×10^{-1} J/cm^2, or to sham irradiation. A minimal erythema dose (MED) of 7.5×10^{-2} J/cm^2 was determined by analyzing skin of wild-type (WT) FVB/N mice 48 h after irradiation (a, n = 5). A comparable MED was observed in wild-type BALB/c mice (b, n = 5). (c,d) Analysis of the skin of *Angptl6/AGF* transgenic mice indicated a MED of 4.0×10^{-2} J/cm^2 of UV-B (d, n = 5), whereas skin of wild-type littermates showed signs of erythema at 7.0×10^{-2} J/cm^2. (e, n = 5) Statistical analysis confirmed that the MED for *Angptl6/AGF* transgenic mice is significantly lower than that of wild-type mice. Data are expressed as mean ± standard deviation (n = 6/condition). ***$P < 0.001$.

Angptl6/AGF promotes blood vessel enlargement in response to a single UV-B exposure

One MED induces formation of an erythema characterized by microvascular enlargement in the skin. Therefore, we asked whether macroscopic vascular enlargement occurs in the skin of *Angptl6/AGF* transgenic mice by irradiating them with increased doses of UV-B. A dose of 9.0×10^{-2} J/cm^2 UV-B induced macroscopic

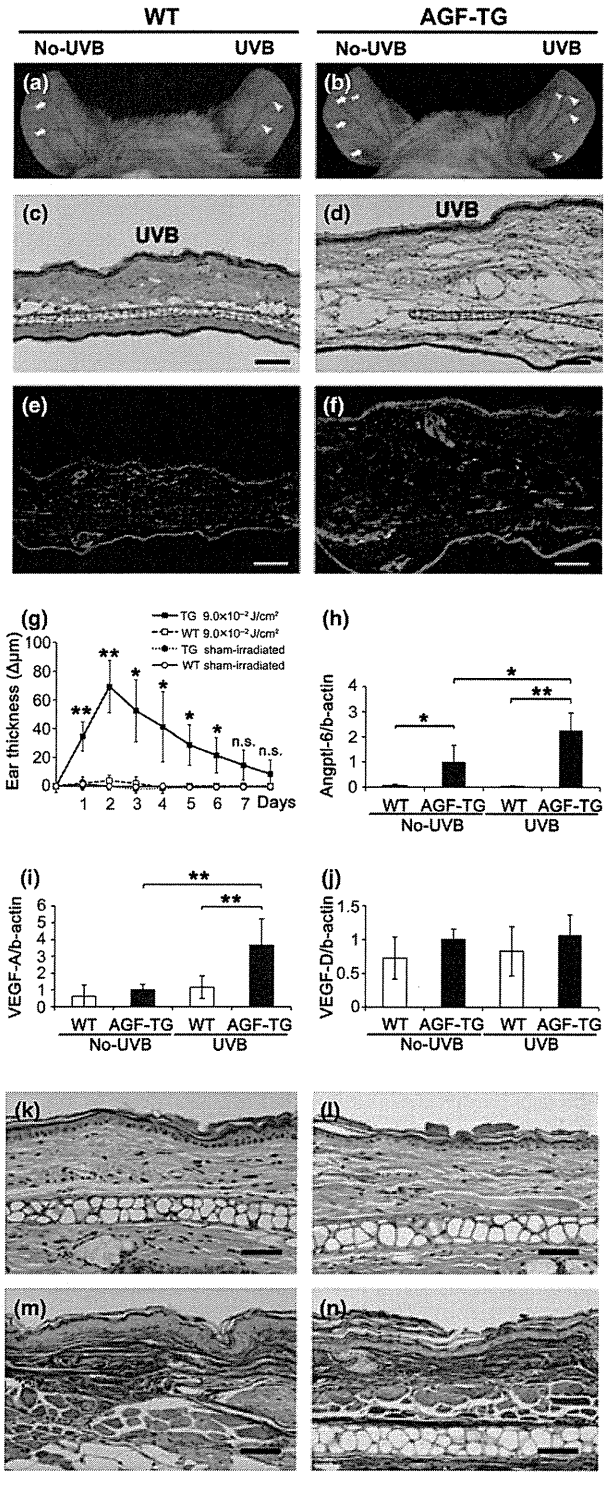

vascular enlargement in ear skin of *Angptl6/AGF* transgenic mice (Fig. 2b, arrowheads) as compared with sham-irradiated ears (Fig. 2b, arrows), whereas no macroscopic vascular alteration was seen in UV-B-exposed (Fig. 2a, arrowheads) or sham-irradiated ear skin of wild-type littermates (Fig. 2a, arrows). Histologically, ear skin of *Angptl6/AGF* transgenic mice showed marked edema in the dermis and vessel dilation 48 h after irradiation (Fig. 2d), whereas the skin of wild-type mice showed no significant changes at 9.0×10^{-2} J/cm^2 UV-B (Fig. 2c). Double immunofluorescence with antibodies against CD31 for blood vessels and LYVE-1 for lymphatic vessels showed that blood vessels were markedly enlarged in *Angptl6/AGF* transgenic mice (Fig. 2f), whereas no such changes were seen in wild-type littermates (Fig. 2e). Lymphatic vessels in *Angptl6/AGF* transgenic mice remained normal as well as lymphatic vessels in wild-type littermates. Furthermore, *Angptl6/AGF* transgenic mice showed prominent, albeit transient, ear swelling 48 h after irradiation (Fig. 2g). In contrast, the ears of wild-type mice showed no detectable changes in thickness after a single UV-B irradiation at 9.0×10^{-2} J/cm^2 (Fig. 2g).

Quantitative real-time RT–PCR analyses of RNA extracted from mouse ears showed that expression levels of Angptl6/AGF and VEGF-A increased by 2.0-fold (Fig. 2h) and 2.5-fold (Fig. 2i), respectively, in *Angptl6/AGF* transgenic mice 48 h after irradiation. By contrast, wild-type mice showed little or no change in expression levels of either transcript after irradiation with 9.0×10^{-2} J/cm^2

Figure 2. Angptl6/AGF promotes blood vessel enlargement following acute ultraviolet (UV)-B irradiation (a,b). The ear skin of *Angptl6/AGF* transgenic (TG) mice or wild-type (WT) littermates was exposed to a single irradiation of UV-B of 9.0×10^{-2} J/cm^2. Forty-eight hours later, transgenic mice developed erythema and enlargement of blood vessels (b, arrowheads) relative to sham-irradiated ears (b, arrows), whereas little or no alteration was observed in UV-B-exposed (a, arrowheads) or sham-irradiated ear skin of wild-type mice (a, arrows). (c,d) Histological analysis revealed that ear skin of wild-type mice appeared normal (c, hematoxylin–eosin [HE]), whereas the skin of Angptl6/AGF-overexpressing mice showed dermal edema and vessel dilation particularly on the side of UV-B irradiation as compared with the other side of ear skin which is unexposed to UV-B (d, HE). (e,f) Double immunofluorescence staining reveals dilated CD31$^+$ blood vessels (red) in transgenic mice, while no such changes were seen in skin of wild-type littermates. LYVE-1$^+$ stain (green) was comparable between ear skin of AGF transgenic mice and wild-type littermates. Nuclei are stained blue (4′,6′-diamidino-2-phenylindole dihydrochloride [DAPI] stain). (Scale bars, 100 μm.) (g) Angptl6/AGF-overexpressing mice show significant ear swelling 48 h after irradiation with 9.0×10^{-2} J/cm^2 UV-B (◆), while no ear swelling is observed in similarly treated wild-type littermates (■). (h–j) Quantitative reverse transcription polymerase chain reaction (RT–PCR) analyses of ear skin of Angptl6/AGF-overexpressing mice and wild-type littermates 48 h after UV-B irradiation (n = 5). Increased Angptl6/AGF and vascular endothelial growth factor (VEGF)-A expression was seen in K14-*Angptl6/AGF* mice in response to a single UV-B exposure (h,i). Comparable levels of VEGF-D mRNA were seen in the presence or absence of UV-B irradiation (j). Routine HE stain showed that ear skin of Angptl6/AGF-overexpressing mice and wild-type mice appeared comparable and normal 8 days after UV-B irradiation (k,l). Azan–Mallory staining showed that collagen bundles in the papillary dermis remained normal in UV-B-treated *Angptl6/AGF* transgenic mice (n) and wild-type littermates 8 days after UV-B irradiation (m). Data are expressed as means ± standard deviation (n = 5/condition and time point). $^{**}P < 0.01$; $^{*}P < 0.05$.

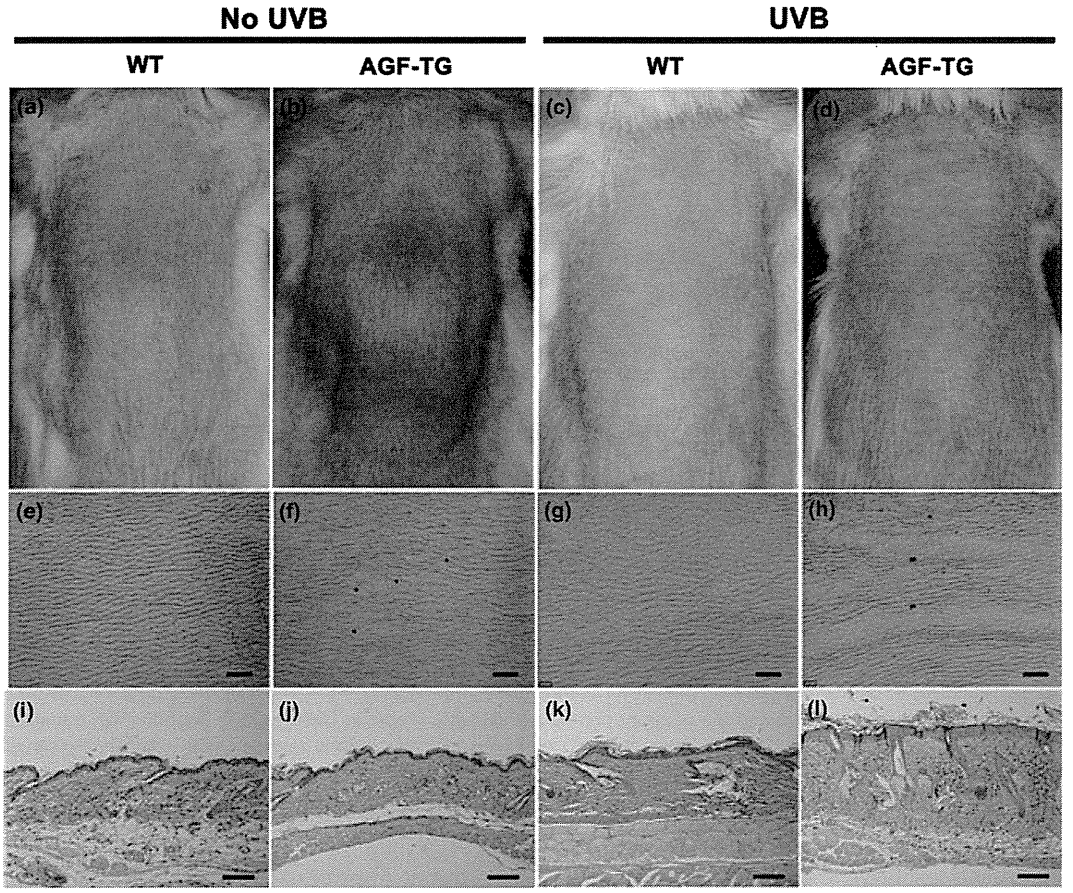

Figure 3. Increased wrinkle formation in Angptl6/AGF-overexpressing mice after long-term ultraviolet (UV)-B irradiation. Dorsal skin of non-irradiated wild-type (WT) and *Angptl6/AGF* transgenic (TG) mice (a,b). After 14 weeks (three times/week) of UV-B irradiation, wild-type mice do not show macroscopic skin alterations (c), whereas *Angptl6/AGF* transgenic mice developed wrinkles and slight erythema (d) (representative images; n = 13/genotype). Skin replicas of wild-type and Angptl6/AGF-overexpressing mice showed no signs of wrinkle formation or texture changes (e,f), nor did those of wild-type mice treated with UV-B (g). Angptl6/AGF-overexpressing mice treated with long-term UV-B irradiation, however, did show wrinkle formation and texture changes (h). (i–l) Hematoxylin–eosin (HE) staining reveals signs of epidermal hyperplasia, edema, inflammatory cell infiltration, and increased vascularization in the papillary dermis in skin of UV-B-irradiated Angptl6/AGF-overexpressing mice (l). The skin of non-irradiated mice of both genotypes (i,j), or of UV-B-irradiated wild-type mice (k) does not show major histological abnormalities. (Scale bars: [e–h] 1 mm, [i–l] 100 μm.)

UV-B. Furthermore, comparable expression levels of VEGF-D were observed in the ears of *Angptl6/AGF* transgenic and wild-type mice under UV-B- or sham-irradiation regimes (Fig. 2j). VEGF-C mRNA levels remained unchanged in either group (data not shown).

To find overall changes of ears in *Angptl6/AGF* transgenic mice and wild-type littermates, we daily measured the ear thickness for 8 days after UV-B irradiation. Seven days after UV-B irradiation, ear thickness was comparable between AGF transgenic mice and wild-type littermates (Fig. 2g). Eight days after UV-B irradiation, the macroscopic appearance of ear skin in *Angptl6/AGF* transgenic mice returned to normal (data not shown). Histologically, ears obtained from *Angptl6/AGF* transgenic mice and wild-type littermates showed comparable cellular morphology 8 days after irradiation based on hematoxylin–eosin staining (Fig. 2k,l). Azan–Mallory staining also indicated little or no degradation of dermal collagen bundles in ears of *Angptl6/AGF* transgenic mice 8 days after irradiation with 9.0×10^{-2} J/cm^2 UV-B (Fig. 2m,n). Together, these results suggest that targeted overexpression of Angptl6/AGF promotes vascular enlargement and subsequent plasma leakage from blood vessels at early stages of UV-B irradiation in murine skin, but that vascular hyperpermeability is not associated with acute photo-induced skin damage.

Angptl6/AGF mediates epidermal hyperplasia in response to chronic UV-B exposure

Overall, we found transient vascular enlargement and reversible ear swelling in *Angptl6/AGF* transgenic mice after a single UV-B exposure but did not observe acute UV-B-induced skin damage or acceleration of the healing process. Therefore, we asked whether targeted Angptl6/AGF overexpression induces skin changes

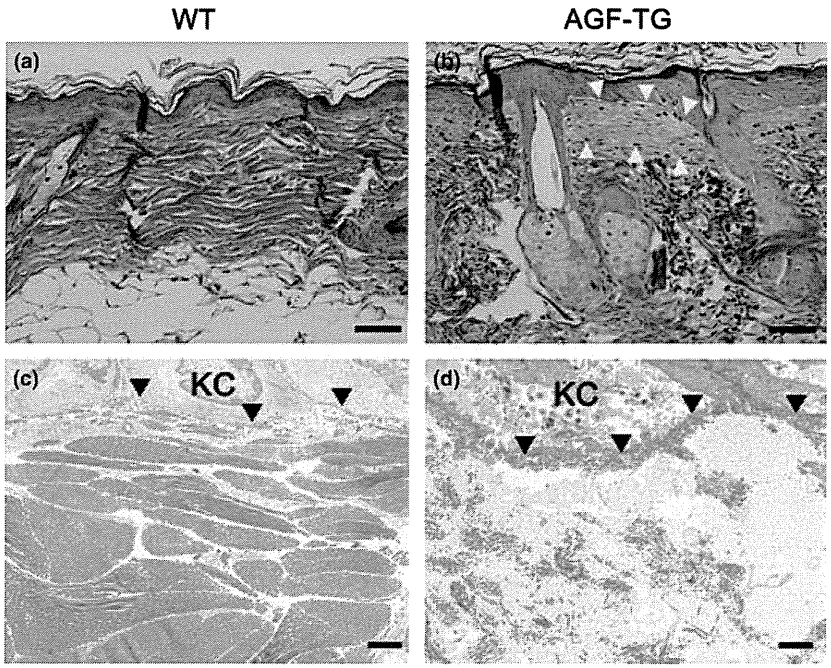

Figure 4. Marked reduction in dermal collagen bundles in *K14–Angptl6/AGF* transgenic mice after long-term ultraviolet (UV)-B. (a,b) Azan–Mallory staining shows that collagen bundles in the papillary dermis are severely altered in UV-B-treated *Angptl6/AGF* transgenic (TG) mice (b, yellows arrows) compared with wild-type (WT) littermates (a). (c,d) Electron micrographs revealed that collagen fibrils and bundles in UV-B-treated AGF transgenic mice were markedly fragmented beneath the dermoepidermal junction (d, arrowheads) compared with wild-type mice (c, arrowheads). (Scale bars: [a,b] 50 μm, [c,d] 2 μm.) KC, keratinocytes.

following chronic UV-B irradiation. *Angptl6/AGF* transgenic mice and wild-type littermates were exposed 3 days a week to a total dose of 8.185 J/cm^2 UV-B for 14 weeks. Wild-type mice showed no skin changes after UV-B irradiation based on both macroscopic appearance (Fig. 3c) and microscopic analysis using skin replicas (Fig. 3g) and appeared comparable in gross appearance to sham-irradiated wild-type mice (Fig. 3a,e). In contrast, the skin of *Angptl6/AGF* transgenic mice exhibited transverse wrinkles after chronic UV-B irradiation (Fig. 3d,h), while sham-irradiated transgenic mice showed little or no wrinkling (Fig. 3b,f). Histologically, the skin of *Angptl6/AGF* transgenic mice showed evidence of epidermal hyperplasia, edema formation and inflammatory cell infiltration in the dermis after chronic UV-B irradiation (Fig. 3l), whereas no such changes were observed in sham-irradiated transgenic mice (Fig. 3j) or in wild-type mice with or without UV-B irradiation (Fig. 3i,k). Azan–Mallory staining showed that the size of collagen bundles was reduced in the upper dermis of *Angptl6/AGF* transgenic mice after chronic UV-B exposure (Fig. 4b), whereas these alterations were not observed in UV-B-irradiated wild-type littermates (Fig. 4a). Moreover, electron microscopic analysis revealed that the regular assembly of collagen was markedly perturbed in the upper dermis of *Angptl6/AGF* transgenic mice after chronic UV-B irradiation (Fig. 4d), whereas the fibrillar collagen network was maintained in the dermis of UV-B-irradiated wild-type mice (Fig. 4c). Together, these results suggest that following chronic UV-B exposure, the skin of *Angptl6/AGF* transgenic mice undergoes alterations leading to wrinkle formation.

Targeted Angptl6/AGF overexpression promotes angiogenesis and lymphatic enlargement in response to chronic UV-B exposure

To determine whether chronic UV-B exposure alters the microvascular network in the skin of *Angptl6/AGF* transgenic mice, we undertook macroscopic and microscopic analyses of blood and lymphatic vessels in the skin. Macroscopic analysis indicated that the skin of transgenic mice was more vascularized after UV-B exposure than that of wild-type littermates either with or without irradiation (Fig. 5a,c,d) or of sham-irradiated transgenic mice (Fig. 5b). Double staining for blood and lymphatic vessels showed that CD31-positive blood vessels were enlarged in the upper dermis of *Angptl6/AGF* transgenic mice after chronic UV-B irradiation (Fig. 5h), whereas few alterations were seen in sham-irradiated transgenic mice or wild-type littermates, either irradiated or not irradiated (Fig. 5e–g). Computer-assisted morphometric analysis of CD31-stained skin sections confirmed that the average number of blood vessels was significantly increased in *Angptl6/AGF* transgenic mice after chronic irradiation (47.23 ± 8.65 blood vessels/mm^2; $P < 0.05$), as compared with sham-irradiated transgenic mice (32.17 ± 3.25 blood vessels/mm^2) or wild-type controls (25.45 ± 3.36 blood vessels/mm^2; Fig. 5j). Furthermore, blood vessels were significantly larger in UV-B-irradiated *Angptl6/AGF* transgenic mice (353.6 ± 41.7 μm^2; $P < 0.05$) than in sham-irradiated transgenic mice (295.6 ± 35.3 μm^2; Fig. 5k). Moreover, we observed a significant increase in the percentage of total tissue area covered by blood vessels in UV-B-irradiated *Angptl6/AGF*

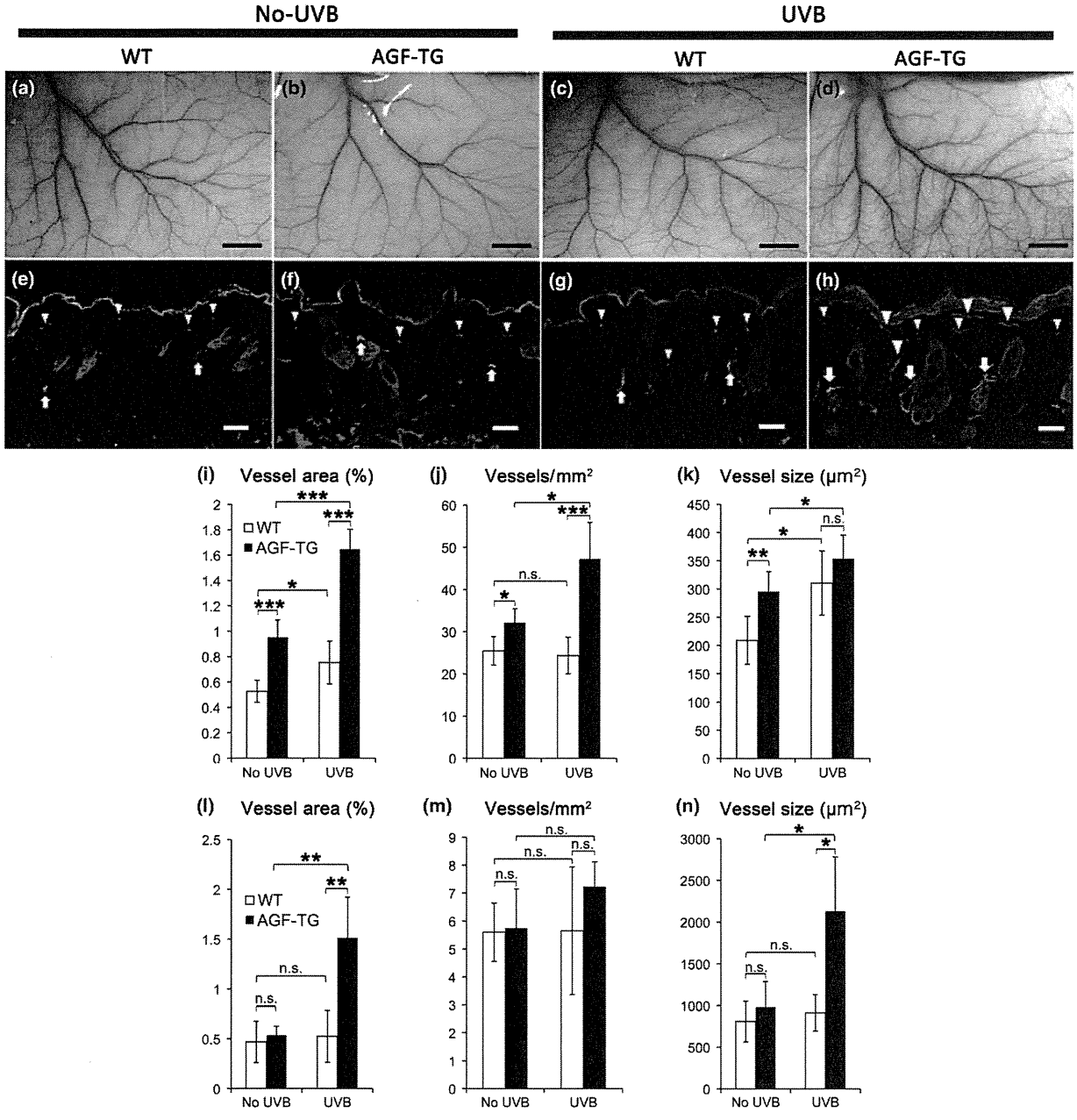

Figure 5. Induction of angiogenesis in *Angptl6/AGF* transgenic (TG) mice after long-term ultraviolet (UV)-B irradiation. (a–d) Increased cutaneous vascularization, with prominent enlargement of blood vessels, is observed after chronic UV-B treatment in the skin of Angptl6/AGF-overexpressing mice (d). Compared with non-irradiated wild-type (WT) littermates (a), no significant changes were observed in wild-type littermates after long-term UV-B irradiation (c) or in Angptl6/AGF-overexpressing mice that did not undergo irradiation (b). (Scale bars: 3 mm.) (e–h) Double immunofluorescence for blood vessels by anti-CD31 antibody (red, arrowheads) and for lymphatic vessels by anti-LYVE-1 antibody (green, arrows) demonstrates prominent vascularization in the dermis of Angptl6/AGF-overexpressing mice after chronic UV-B irradiation (h), whereas few vessels were altered in wild-type littermates that did or did not undergo UV-B irradiation (e,g) and in non-irradiated Angptl6/AGF-overexpressing mice (f). (Scale bars, 50 μm.) (i) Computer-assisted morphometric analysis of CD31-stained skin sections after 14 weeks of UV-B irradiation revealed a significant increase in the relative area occupied by blood vessels (i) and in blood vessel density (j) in *Angptl6/AGF* transgenic mice (■) compared with wild-type littermates (□). (k) Enlargement of blood vessels detected by CD31 staining is prominent in UV-B-treated *Angptl6/AGF* transgenic mice. Skin sections after 14 weeks of UV-B irradiation show a significant increase in the relative area occupied by lymphatic vessels (l) and in average vessel size (n) in *Angptl6/AGF* transgenic mice (■) compared with wild-type mice. In contrast, no significant differences were observed in the vessel density (m) between non-irradiated and irradiated skin of AGF transgenic mice (■) and wild-type littermates (□). Data are expressed as mean ± standard deviation ($n = 5$). ***$P < 0.001$; **$P < 0.01$; *$P < 0.05$.

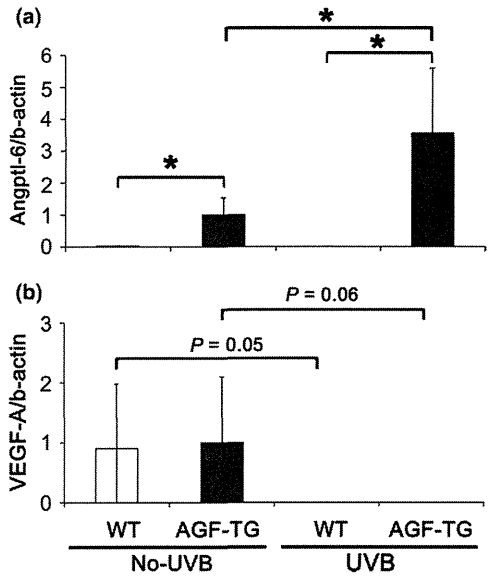

Figure 6. Chronic ultraviolet (UV)-B exposure promotes increased levels of Angptl6/AGF mRNA and decreased levels of vascular endothelial growth factor (VEGF)-A mRNA. (a) Angptl6/AGF mRNA levels were significantly increased in the skin of UV-B-exposed transgenic (TG) mice compared with wild-type littermates. (b) In contrast, VEGF-A mRNA expression in the skin was undetectable after UV-B irradiation of either wild-type or *Angptl6/AGF* transgenic mice.

transgenic mice (1.65 ± 0.16%) compared with controls (0.75 ± 0.17%; $P < 0.001$) (Fig. 5i). Lymphatic-specific staining with LYVE-1 revealed marked enlargement of dermal lymphatic vessels in UV-B-irradiated skin of *Angptl6/AGF* transgenic mice (Fig. 5h) compared with sham-irradiated transgenic mice (Fig. 5f) or irradiated or non-irradiated wild-type mice (Fig. 5e,g). Computer-assisted morphometric analysis showed that the size of dermal lymphatic vessels is significantly increased by twofold ($P < 0.05$) in *Angptl6/AGF* transgenic mice after chronic UV-B irradiation (2129.2 ± 654.1 μm^2; $P < 0.05$) compared with non-irradiated transgenic mice (981.5 ± 305.4 μm^2), or wild-type controls with or without UV-B irradiation (911.2 ± 219.3 μm^2 or 807.7 ± 242.6 μm^2, respectively; Fig. 5n). The percentage of total tissue area covered by lymphatic vessels of *Angptl6/AGF*-overexpressing skin was significantly increased after chronic UV-B-irradiation (1.51 ± 0.41%; $P < 0.001$) compared with sham-irradiated *Angptl6/AGF* transgenic mice (0.53 ± 0.09%) or wild-type controls with or without UV-B irradiation (0.52 ± 0.26% or 0.47 ± 0.21%, respectively; Fig. 5l). However, the average density of dermal lymphatics in both genotypes with or without chronic UV-B exposure was comparable (Fig. 5m). Importantly, increased levels of ectopic *Angptl6/AGF* mRNA were observed in UV-B-exposed skin of *Angptl6/AGF* transgenic mice as compared with sham-irradiated skin of transgenic mice (Fig. 6). No changes in VEGF-A mRNA levels were observed in UV-B-exposed skin of either *Angptl6/AGF* transgenic or wild-type mice (Fig. 6). Together, these results suggest that overexpression of *Angptl6/AGF* in mouse skin promotes prominent angiogenesis and subsequent enlargement of lymphatic vessels.

DISCUSSION

In this study, we subjected *Angptl6/AGF* transgenic mice to UV-B exposure, a major risk for cutaneous damage, to test the hypothesis that Angptl6/AGF might reduce acute and/or chronic skin damage by accelerating tissue repair. Interestingly, however, our results indicate that chronic UV-B activates the K14 promoter driving the Angptl6/AGF transgene, resulting in photo-induced skin alterations at a subthreshold UV-B dose that induced little or no skin changes in wild-type littermates.

Recent studies indicate that UV-B potently induces an angiogenic switch, namely, upregulates pro-angiogenic mediators and downregulates anti-angiogenic ones, leading to a pathological pro-angiogenic condition in the skin.[9] In support of this concept, targeted VEGF-A overexpression in mouse skin was shown to promote vascular enlargement and subsequent vascular leakage in response to a single UV-B exposure.[9] In addition, VEGF-A transgenic mice showed increased inflammatory cell infiltration in the dermis and epidermal hyperplasia at subthreshold UV-B doses, features typical of acute UV-B-induced skin damage.[9] In contrast, in the present study, targeted Angptl6/AGF overexpression in mouse skin promoted little or no epidermal hyperplasia in response to a single UV-B exposure, although marked enlargement of cutaneous blood vessels was observed. In fact, Angptl6/AGF has been shown to increase the vascular network of capillary-sized blood vessels in a physiological pattern,[17] whereas VEGF-A induces formation of tortuous, capillary-sized blood vessels in transgenic mice, leading to promotion of leukocyte trafficking and rolling.[20] Therefore, physiological induction of AGF by a single UV-B exposure may prevent enhanced vascular leakage, which would initiate cutaneous inflammation and subsequent epidermal hyperplasia.

In contrast to a single UV-B exposure, chronic UV-B exposure over 14 weeks was accompanied by prominent skin alterations, including epidermal hyperplasia, in *Angptl6/AGF* transgenic mice as compared with wild-type littermates. Overproduction of AGF over a long period may underlie the development of wrinkles seen in response to chronic UV-B irradiation. In fact, in this study, a total dose of 8.156 J/cm^2 UV-B was required to promote development of macroscopic wrinkles in *K14–Angptl6/AGF* transgenic mice, whereas a total dose of 0.72 J/cm^2 UV-B was sufficient to induce chronic photo-induced skin damage in irradiated *K14–VEGF-A* transgenic mice.[9] Interestingly, no induction of VEGF-A mRNA was found in *Angptl6/AGF* transgenic mice which were exposed to the long-term UV-B irradiation in the skin, whereas *Angptl6/AGF* mRNA levels were significantly increased in those mice. Therefore, these findings suggest that long-term UV-B irradiation activates the K14 promoter driving the *Angptl6/AGF* transgene, and that the ectopic overexpression of AGF actively promotes the development of chronic photo-induced skin alterations in an independent manner.

Dermal lymphatic vessels were markedly enlarged in *Angptl6/AGF* transgenic mice after chronic UV-B exposure. In contrast, little or no lymphatic vessel alteration was seen in sham-irradiated *Angptl6/AGF* transgenic mice compared with wild-type littermates. Does experimental induction of Angptl6/AGF by chronic UV-B exposure mediate dilation of lymphatic vessels? The skin of

UV-B-exposed *Angptl6/AGF* transgenic mice exhibits signs of enhanced angiogenesis reflected by an increased number of blood vessels compared to sham-irradiated mice. In contrast, the density of lymphatic vessels was comparable between chronic UV-B- and sham-irradiated *Angptl6/AGF* mice, suggesting that Angptl6/AGF does not induce lymphangiogenesis as it does angiogenesis. However, increased blood flow can induce uptake and subsequent transport of fluids by dermal lymphatic vessels, likely promoting significant enlargement of the lymphatic vasculature. Importantly, chronic UV-B exposure markedly upregulated Angptl6/AGF mRNA levels, whereas no upregulation of VEGF-A mRNA levels was observed in this model. VEGF-A, but not VEGF-C or VEGF-D, was previously shown to be upregulated in *hairless* mice in response to chronic UV-B exposure, an effect accompanied by enlargement and impairment of lymphatic vessels.[14] Furthermore, functional inactivation of VEGF-A inhibits enlargement of lymphatic vessels after a single UV-B exposure, suggesting that VEGF-A is responsible for both vascular hyperpermeability and reduced lymphatic drainage in response to UV-B exposure.[14] Therefore, angiogenesis and increased blood flow likely promote enlargement of lymphatic vessels and alter their function in chronic UV-B-induced skin damage. Accordingly, Angptl6/AGF has been recently shown to enhance blood flow in a mouse hind-limb ischemia model.[21] In addition, epidermal overexpression of Angptl2 promotes marked enlargement of lymphatic and blood vessels in the skin. Moreover, sufficient lymphatic flow is required to minimize tissue edema and subsequent inflammation in response to UV-B irradiation.[22] Therefore, future studies should address whether UV-B irradiation alters lymphatic flow and/or function in Angptl transgenic mice, and whether metastasis associated with UV-B-induced carcinogenesis is correlated with changes in lymphatic vessel function.

ACKNOWLEDGMENTS

The authors thank Mika Ikeda, Eriko Tan and Teruko Tsuda for technical assistance. The Japanese Society for Investigative Dermatology Fellowship SHISEIDO Award 2008 (to S. H.), and a Grant-in-Aid for Scientific Research from the Ministry of Education, Culture, Sports, Science, and Technology of Japan (to Y. N.).

REFERENCES

1 Folkman J. Tumor angiogenesis: therapeutic implications. *N Eng J Med* 1971; **285**: 1182–1186.
2 Dvorak HF, Brown LF, Detmar M, Dvorak AM. Vascular permeability factor/vascular endothelial growth factor, microvascular hyperpermeability, and angiogenesis. *Am J Pathol* 1995; **146**: 1029–1239.
3 Kligman LH. Symposium on models for the study of human photoaging: American Society for Photobiology. *Photochem Photobiol* 1989; **50**: 903–905.
4 Yano K, Oura H, Detmar M. Targeted overexpression of the angiogenesis inhibitor thrombospondin-1 in the epidermis of transgenic mice prevents ultraviolet-B-induced angiogenesis and cutaneous photo-damage. *J Invest Dermatol* 2002; **118**: 800–805.
5 Yano K, Kadoya K, Kajiya K, Hong YK, Detmar M. Ultraviolet B irradiation of human skin induces an angiogenic switch that is mediated by upregulation of vascular endothelial growth factor and by downregulation of thrombospondin-1. *Br J Dermatol* 2005 (Jan); **152** (1): 115–121.
6 Kramer M, Sachsenmaier C, Herrlich P, Rahmsdorf HJ. UV irradiation-induced interleukin-1 and basic fibroblast growth factor synthesis and release mediate part of the UV response. *J Biol Chem* 1993; **268**: 6734–6741.
7 Strickland I, Rhodes LE, Flanagan BF, Friedmann PS. TNF-alpha and IL-8 are upregulated in the epidermis of normal human skin after UVB exposure: correlation with neutrophil accumulation and E-selectin expression. *J Invest Dermatol* 1997; **108**: 763–768.
8 Bielenberg DR, Bucana CD, Sanchez R, Donawho CK, Kripke ML, Fidler IJ. Molecular regulation of UVB-induced cutaneous angiogenesis. *J Invest Dermatol* 1998; **111**: 864–872.
9 Hirakawa S, Fujii S, Kajiya K, Yano K, Detmar M. Vascular endothelial growth factor promotes sensitivity to ultraviolet B-induced cutaneous photodamage. *Blood* 2005; **105**: 2392–2399.
10 Oike Y, Ito Y, Maekawa H *et al.* Angiopoietin-related growth factor (AGF) promotes angiogenesis. *Blood* 2004; **103**: 3760–3765.
11 Oike Y, Akao M, Yasunaga K *et al.* Angiopoietin-related growth factor antagonizes obesity and insulin resistance. *Nat Med* 2005; **11**: 400–408.
12 Hato T, Tabata M, Oike Y. The role of angiopoietin-like proteins in angiogenesis and metabolism. *Trends Cardiovasc Med* 2008 (Jan); **18** (1): 6–14.
13 Oike Y, Yasunaga K, Ito Y *et al.* Angiopoietin-related growth factor (AGF) promotes epidermal proliferation, remodeling, and regeneration. *Proc Natl Acad Sci USA* 2003; **100**: 9494–9499.
14 Kajiya K, Hirakawa S, Detmar M. Vascular endothelial growth factor-A mediates ultraviolet B-induced impairment of lymphatic vessel function. *Am J Pathol* 2006; **169**: 1496–1503.
15 Hirakawa S, Detmar M. New insights into the biology and pathology of the cutaneous lymphatic system. *J Dermatol Sci* 2004 (Jun); **35** (1): 1–8.
16 Kajiya K, Sawane M, Huggenberger R, Detmar M. Activation of the VEGFR-3 pathway by VEGF-C attenuates UVB-induced edema formation and skin inflammation by promoting lymphangiogenesis. *J Invest Dermatol* 2009; **129**: 1292–1298.
17 Tabata M, Kadomatsu T, Fukuhara S *et al.* Angiopoietin-like protein 2 promotes chronic adipose tissue inflammation and obesity-related systemic insulin resistance. *Cell Metab* 2009; **10**: 178–188.
18 Hirakawa S, Kodama S, Kunstfeld R, Kajiya K, Brown LF, Detmar M. VEGF-A induces tumor and sentinel lymph node lymphangiogenesis and promotes lymphatic metastasis. *J Exp Med* 2005; **201**: 1089–1099.
19 Hirakawa S, Detmar M, Kerjaschki D *et al.* Nodal lymphangiogenesis and metastasis: role of tumor-induced lymphatic vessel activation in extramammary Paget's disease. *Am J Pathol* 2009; **175**: 2235–2248.
20 Detmar M, Brown LF, Schön MP *et al.* Increased microvascular density and enhanced leukocyte rolling and adhesion in the skin of VEGF transgenic mice. *J Invest Dermatol* 1998; **111**: 1–6.
21 Urano T, Ito Y, Akao M *et al.* Angiopoietin-related growth factor enhances blood flow via activation of the ERK1/2-eNOS-NO pathway in a mouse hind-limb ischemia model. *Arterioscler Thromb Vasc Biol* 2008; **28**: 827–834.
22 Kajiya K, Detmar M. An important role of lymphatic vessels in the control of UVB-induced edema formation and inflammation. *J Invest Dermatol* 2006; **126**: 919–921.

The American Journal of Pathology, Vol. 181, No. 6, December 2012

http://dx.doi.org/10.1016/j.ajpath.2012.08.023

Vascular Biology, Atherosclerosis, and Endothelium Biology

Topical Simvastatin Accelerates Wound Healing in Diabetes by Enhancing Angiogenesis and Lymphangiogenesis

Jun Asai,* Hideya Takenaka,* Satoshi Hirakawa,† Jun-ichi Sakabe,† Asami Hagura,* Saburo Kishimoto,* Kazuichi Maruyama,‡ Kentaro Kajiya,§ Shigeru Kinoshita,‡ Yoshiki Tokura,† and Norito Katoh*

From the Departments of Dermatology and Ophthalmology,‡ Graduate School of Medical Science, Kyoto Prefectural University of Medicine, Kyoto; the Department of Dermatology,† Hamamatsu University School of Medicine, Hamamatsu; and the Shiseido Innovative Science Research Center,§ Yokohama, Japan*

Impaired wound healing is a major complication of diabetes. Recent studies have reported reduced lymphangiogenesis and angiogenesis during diabetic wound healing, which are thought to be new therapeutic targets. Statins have effects beyond cholesterol reduction and can stimulate angiogenesis when used systemically. However, the effects of topically applied statins on wound healing have not been well investigated. The present study tested the hypothesis that topical application of simvastatin would promote lymphangiogenesis and angiogenesis during wound healing in genetically diabetic mice. A full-thickness skin wound was generated on the back of the diabetic mice and treated with simvastatin or vehicle topically. Simvastatin administration resulted in significant acceleration of wound recovery, which was notable for increases in both angiogenesis and lymphangiogenesis. Furthermore, simvastatin promoted infiltration of macrophages, which produced vascular endothelial growth factor C in granulation tissues. *In vitro*, simvastatin directly promoted capillary morphogenesis and exerted an antiapoptotic effect on lymphatic endothelial cells. These results suggest that the favorable effects of simvastatin on lymphangiogenesis are due to both a direct influence on lymphatics and indirect effects via macrophages homing to the wound. In conclusion, a simple strategy of topically applied simvastatin may have significant therapeutic potential for enhanced wound healing in patients with impaired microcirculation such as that in diabetes. *(Am J Pathol 2012, 181:2217–2224; http://dx.doi.org/10.1016/j.ajpath.2012.08.023)*

Delayed wound healing is a major complication of diabetes and is caused by increased apoptosis, delayed cellular infiltration, reduced angiogenesis, and decreased formation and organization of collagen fibers.[1–3] Impaired lymphangiogenesis has also recently been established as a major factor in diabetic refractory wound healing.[4,5] The functions of lymphatic vessels in wounds are to drain the protein-rich lymph from the extracellular space, to maintain normal tissue pressure, and to mediate the immune response.[6,7] Delayed wound healing, such as that seen in infections, appears to result from persistent edema and delayed removal of debris and inflammatory cells due to reduced lymphatic development.[8]

Statins are HMG-CoA (5-hydroxy-3-methylglutaryl-coenzyme A) reductase inhibitors that are primarily used to lower circulating cholesterol levels. In addition, statins have been found to protect against ischemic injury and stimulate angiogenesis in normocholesterolemic animals.[9–11] This angiogenic effect is partially mediated by direct regulation of proliferation of endothelial cells and capillary morphogenesis via the Akt/PI3K pathway.[11] Simvastatin has been found to enhance vascular endothelial growth factor (VEGF) production and improve wound healing in an experimental model of diabetes,[12] and nitropravastatin stimulates reparative neovascularization and improves recovery from limb ischemia in type 1 diabetic mice.[13] However, systemic administration at an extremely high dose was used to obtain angiogenic effects in

Supported by grants from the Ministry of Education, Culture, Sports, Science and Technology of Japan.

Accepted for publication August 15, 2012.

CME Disclosure: The authors of this article and the planning committee members and staff have no relevant financial relationships with commercial interest to disclose.

Supplemental material for this article can be found at *http://ajp.amjapathol.org* or at *http://dx.doi.org/10.1016/j.ajpath.2012.08.023*.

Address reprint requests to Jun Asai, M.D., Ph.D., Department of Dermatology, Graduate School of Medical Science, Kyoto Prefectural University of Medicine, 465 Hirokoji, Kawaramachi, Kamigyo-Ku, Kyoto, 602-8566, Japan. E-mail: jasai@koto.kpu-m.ac.jp.

these studies, and this is inapplicable for clinical use as an angiogenic drug in patients with ischemic disorders. However, topical application of statins with avoidance of systemic adverse effects may be useful for cutaneous wound healing, in which angiogenesis plays a pivotal role.[14] The lymphangiogenic effects of statins have not been widely investigated. In this study, we evaluated the effects of topical simvastatin on angiogenesis and lymphangiogenesis in a mouse model of impaired diabetic wound healing.

Materials and Methods

Animals

Genetically diabetic C57BLKS/J-m+/+*Lepr*^{db} mice (db/db mice) were obtained from Clea Japan, Inc. (Tokyo, Japan). All procedures were performed in accordance with the guidelines of the Animal Care and Use Committees of Kyoto Prefectural University of Medicine.

Creation of Wounds

Mice were between 6 and 10 weeks old at the time of the study. Wounds were generated as described previously.[15–17] In brief, after induction of deep anesthesia by i.p. injection of sodium pentobarbital (160 mg/kg), full-thickness, excisional skin wounds using 8-mm skin biopsy punches were made on the backs of mice, with one wound generated in each mouse. Each wound was covered with a semipermeable polyurethane dressing (OpSite; Smith and Nephew, Massillon, OH) after topical application of simvastatin (Calbiochem, La Jolla, CA) in petroleum jelly (a mixture of 5 mg of simvastatin and 995 mg of jelly) or vehicle (petroleum jelly alone). Simvastatin in petroleum jelly (10 mg of the mixture containing 50 μg of simvastatin) or vehicle were applied to the wound on days 0, 4, 7, and 10 after creation of the wound.

Monitoring of Wound Healing

A total of 5 db/db mice were used at each time point. Wound healing was monitored by taking pictures with a digital camera (Nikon Coolpix 995; Nikon, Tokyo, Japan) on days 0, 4, 7, and 14 after wound creation. Images were analyzed using ImageJ software version 1.46 (NIH, Bethesda, MD)[18] by tracing the wound margin with a high-resolution computer mouse and calculating the pixel area. Wound closure was calculated as follows: Percentage Closed = [(Area on Day 0 − Open Area on Final Day)/Area on Day 0] × 100, as described previously.[15] The areas of the wounds were compared with Student's *t*-test with $P < 0.05$ taken to indicate a significant difference.

Histologic Score

A histologic score was assigned in a masked manner as described previously.[15] Briefly, each specimen received a score of 1 to 12 as follows: 1 to 3, none to minimal cell accumulation and granulation tissue or epithelial migration; 4 to 6, thin, immature granulation dominated by inflammatory cells but with few fibroblasts, capillaries, or collagen deposition and minimal epithelial migration; 7 to 9, moderately thick granulation tissue, ranging from mainly inflammatory cells to more fibroblasts and collagen deposition; and 10 to 12, thick, vascular granulation tissue dominated by fibroblasts and extensive collagen deposition.

Evaluation of Wound Angiogenesis and Lymphangiogenesis

Sections were stained with rat anti-CD31 antibody (1:100) (BD Biosciences, San Jose, CA) or rabbit anti-LYVE-1 antibody (Upstate, Lake Placid, NY). Green fluorescence was generated by labeling with fluorescein isothiocyanate (FITC)–streptavidin (Vector Laboratories, Burlingame, CA) and biotinylated anti-rat or anti-rabbit antibody (both Vector Laboratories). Wound angiogenesis or lymphangiogenesis was analyzed by calculating the percentage of fluorescent area.[16,19] Briefly, for each slide, an image of the granulation tissue at the wound margin was captured. ImageJ software was used to quantitate the fluorescence intensity. The mean percentage of fluorescent pixels of five images served as an index of the angiogenic or lymphangiogenic response.

Evaluation of Macrophage Number, Phenotype, and VEGF-C Expression in Granulation Tissue

Sections of wounds were stained with rat anti-F4/80 antibody (Invitrogen, Carlsbad, CA). Labeling with F4/80 was visualized with Cy3-conjugated anti-rat antibody (Vector Laboratories). Ten granulation tissue fields (two sections from each animal) were selected, and F4/80-positive cells were counted.[16] VEGF-C expression was evaluated using goat anti-VEGF-C antibody (Santa Cruz Biotechnology, Santa Cruz, CA) and FITC-conjugated anti-goat antibody (Vector Laboratories). To determine the phenotype of infiltrating macrophages, IL-13 and tumor necrosis factor (TNF) α expression was evaluated using goat anti-IL-13 antibody and goat anti-TNF-α antibody (Santa Cruz Biotechnology), respectively, and FITC-conjugated anti-goat antibody. F4/80-positive TNF-α–positive cells were defined as an M1 phenotype and F4/80-positive IL-13–positive cells as an M2 phenotype. In each slide, F4/80-positive cells, F4/80-positive TNF-α–positive cells, and F4/80-positive IL-13–positive cells were counted, and percentages of TNF-α–positive macrophages and IL-13–positive macrophages were evaluated. The mean percentages of TNF-α–positive macrophages and IL-13–positive macrophages in five images were used as indexes of the M1 and M2 phenotypes, respectively.

RNA Isolation, cDNA Synthesis, and Quantitative RT-PCR

Tissue sections obtained in RNAlater (Ambion, Paisley, UK) were processed for RNA isolation, cDNA synthesis, and quantitative RT-PCR.[16] VEGF-C, fibroblast growth factor 2, endothelial nitric oxide synthase, stromal cell-derived factor 1α, and platelet-derived growth factor β gene expression levels were normalized based on the level of an internal

reference gene, 18S. The primers used in the study were obtained from QIAGEN (Düsseldorf, Germany).

Cell Culture

Primary human lymphatic endothelial cells (LECs) were collected as previously described.[20] LECs were cultured at 37°C in 5% CO_2 in endothelial cell basal medium 2 (Lonza, Walkersville, MD) supplemented with 5% fetal bovine serum, human VEGF-A, human fibroblast growth factor 2, human epidermal growth factor, insulin-like growth factor 1, and ascorbic acid. Each experiment was conducted at least three times, with similar results. A representative experiment is shown.

Western Blot Analysis

Cells were lysed with RIPA buffer (Invitrogen) and sonicated. After sonication, cell lysates were centrifuged at 15,400 × *g* for 20 minutes at 4°C, and the supernatants were collected into fresh tubes. Then 4× SDS sample buffer with 0.1 mol/L dithiothreitol was added to samples. Samples were boiled for 5 minutes at 95°C, and 20-μg extracts were separated by 10% SDS-PAGE and electroblotted onto polyvinylidene difluoride membranes for 2 hours at 180 mA. The membranes were incubated with rabbit anti-human Akt (pan) (C67E7) monoclonal antibody (Cell Signaling Technology, Danvers, MA), rabbit anti-human phospho-Akt (Ser473) (D9E) monoclonal antibody (Cell Signaling Technology), or mouse anti-GAPDH monoclonal antibody (Santa Cruz Biotechnology) and detected with horseradish peroxidase–conjugated goat anti-rabbit IgG (Bio-Rad, Hercules, CA) or horseradish peroxidase–conjugated goat anti-mouse IgG (Bio-Rad). Immunoblots were visualized using an ECL Plus Western Blotting Detection Reagents Kit (GE Healthcare, Little Chalfont, Buckinghamshire, UK) according to the manufacturer protocol.

Chord Formation Assay

LECs were used in a chord formation assay.[21] An aliquot (100 μL) of growth factor–depleted Matrigel (Becton Dickinson, Bedford, MA) was added to a 24-well dish and allowed to gel for 30 minutes at 37°C. LECs were seeded at 5×10^4 cells/mL in 500 μL of endothelial cell basal medium 2 containing 3% fetal bovine serum. Cells were cultured in the absence or presence of various doses of simvastatin (Calbiochem, Darmstadt, Germany) with or without pretreatment with a PI3 kinase inhibitor, LY294002 (50 μmol/L) (ENZO Life Sciences, Plymouth Meeting, PA), the mTOR/raptor inhibitor rapamycin (100 nmol/L) (Merck Millipore, Darmstadt, Germany), or the PI3K/mTOR inhibitor wortmannin-rapamycin (100 nmol/L) (Cayman Chemical, Ann Arbor, MI) for 30 minutes. Chord formation was monitored for 24 hours. Digital pictures were taken using a spot image analysis system, and the total length of the chord-like structures at 12 hours was outlined and measured using ImageJ software.

Proliferation Assay

The proliferative activity of cells treated with simvastatin was examined using a CellTiter 96 nonradioactive cell proliferation assay (Promega, Madison, WI). Briefly, subconfluent cells (5000 cells per well) were reseeded on 96-well, flat-bottomed plates with 100 μL of growth media. The cells were treated with simvastatin and incubated for 48 hours at 37°C. Absorbance at 570 nm was recorded using a 96-well enzyme-linked immunosorbent assay (ELISA) plate reader.

Apoptosis Assay

An apoptosis assay was performed using a DeadEnd Fluorometric TUNEL System (Promega). Briefly, LECs were plated on chamber slides and placed in medium. Cells were stimulated by simvastatin and incubated for 24 hours with medium containing 400 μmol/L H_2O_2. To quantify apoptosis, 400 nuclei from random microscopic fields were analyzed by an observer masked to the treatment groups. The number of apoptotic cells was expressed as a percentage of the total cell count.

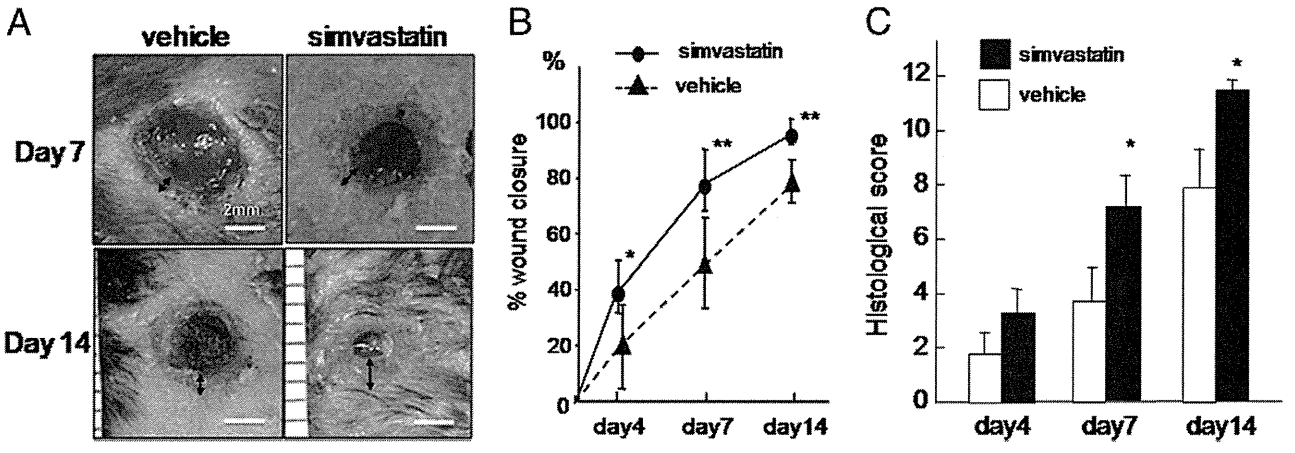

Figure 1. Effects of topical simvastatin on wound closure and histologic score in db/db mice. **A:** Representative macroscopic views of wounds after different treatments and periods. Scale bar = 2 mm. **Arrows** indicate the epithelialized range. **B:** Wound closure was measured on days 4, 7, and 14. $^*P < 0.05$, $^{**}P < 0.001$ versus vehicle ($n = 5$ in each group). **C:** Histologic scores for days 4, 7, and 14, quantified as described in *Materials and Methods*. Higher histologic scores indicate a greater extent of wound healing. $^*P < 0.05$ versus vehicle ($n = 5$ in each group).

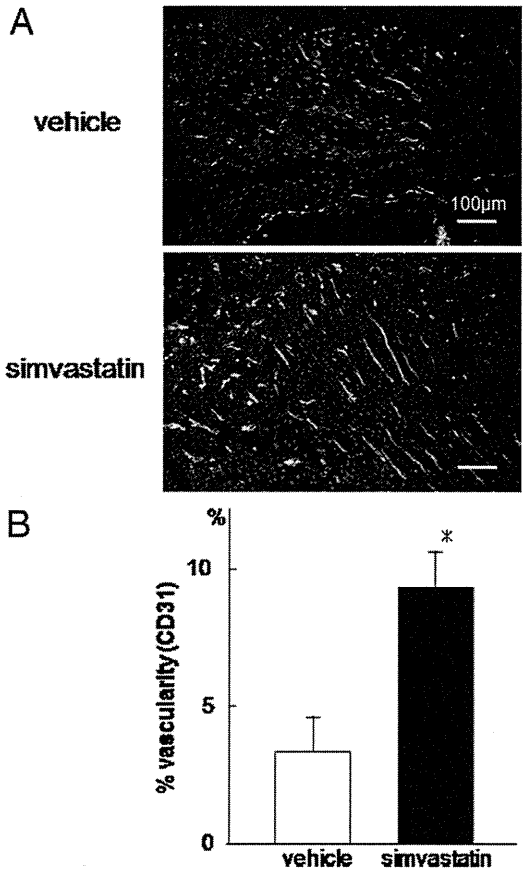

Figure 2. Effects of simvastatin on vascularity in granulation tissues at the wound margin in db/db mice. **A:** Neovascularization at the wound margin in simvastatin- or vehicle-treated diabetic mice after 14 days. Original magnification, ×100. Scale bar = 100 μm. Green and blue fluorescence corresponds to CD31-positive newly formed blood vessels and DAPI-labeled nuclei, respectively. **B:** Percentage of vascularity, quantified as described in *Materials and Methods*. *$P < 0.001$ versus vehicle ($n = 5$ in each group).

Statistical Analysis

All results are presented as mean ± SEM. Statistical comparisons between two groups were performed by Student's *t*-test. Multiple groups were analyzed by one-way analysis of variance followed by appropriate post hoc tests to determine statistical significance. $P < 0.05$ was considered significant. All *in vitro* experiments were performed at least in triplicate.

Results

Simvastatin Accelerates Wound Healing in Diabetic Mice

Wound areas on days 7 and 14 in simvastatin- or vehicle-treated diabetic mice are shown in Figure 1A. On day 14, simvastatin-treated wounds had more than 90% epithelialization, whereas <80% of the wound was epithelialized in the vehicle-treated group (Figure 1B). Simvastatin treatment resulted in significantly smaller wound areas after 4, 7, and 14 days. The difference in percentage of wound closure reached a maximum on day 7 (simvastatin versus control: 79.26% ± 11.09% versus 52.45% ± 16.81%; $P < 0.001$). The histologic score reflects the degree of maturation of granulation tissue, including inflammation, collagen deposition, and reepithelialization, in addition to neovascularization; therefore, higher histologic scores reflect a greater extent of wound healing. The histologic scores for wounds treated with simvastatin were significantly higher than those in the vehicle-treated group (day 4: 3.6 ± 0.70 versus 1.9 ± 0.73; day 7: 7.3 ± 0.94 versus 3.7 ± 0.94, $P < 0.01$; day 14: 11.6 ± 0.51 versus 8.0 ± 1.15, $P < 0.01$)(Figure 1C).

Simvastatin Promotes Both Angiogenesis and Lymphangiogenesis

Wound angiogenesis was analyzed by immunostaining of an endothelial cell–specific marker, CD31, in 10-μm frozen sections to visualize neovascularization. Figure 2A shows neovascularization at the margin in simvastatin- or vehicle-treated wounds in diabetic mice on day 14. A few small vessels were seen at the wound margin in the vehicle-treated group, whereas large numbers of vessels were growing toward the center of the wound in the

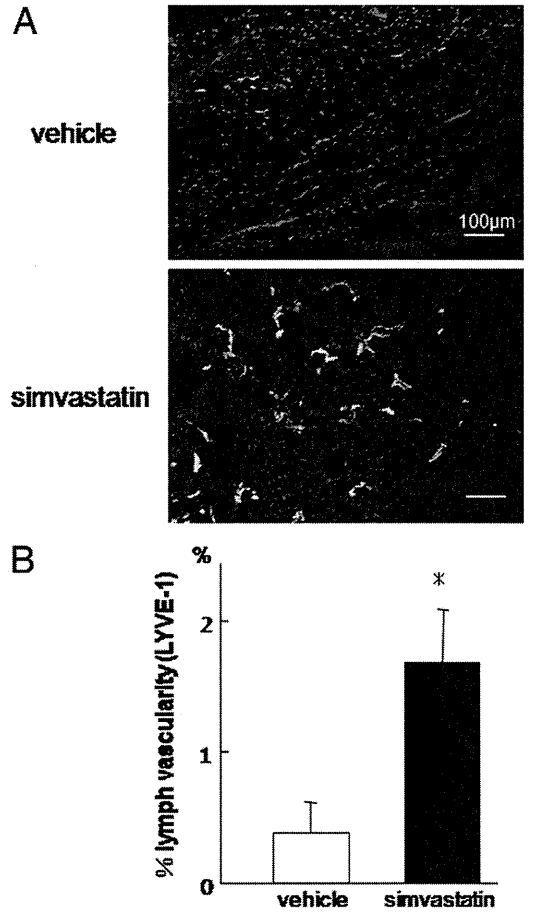

Figure 3. Effects of simvastatin on lymphangiogenesis in granulation tissues at the wound margin in db/db mice. **A:** Lymphangiogenesis at the wound margin in simvastatin- or vehicle-treated diabetic mice after 14 days. Original magnification, ×100. Scale bar = 100 μm. Green and blue fluorescence corresponds to LYVE-1–positive newly formed lymphatic vessels and DAPI-labeled nuclei, respectively. **B:** Percentage of lymphatic vascularity, quantified as described in *Materials and Methods*. *$P < 0.001$ versus vehicle ($n = 5$ in each group).

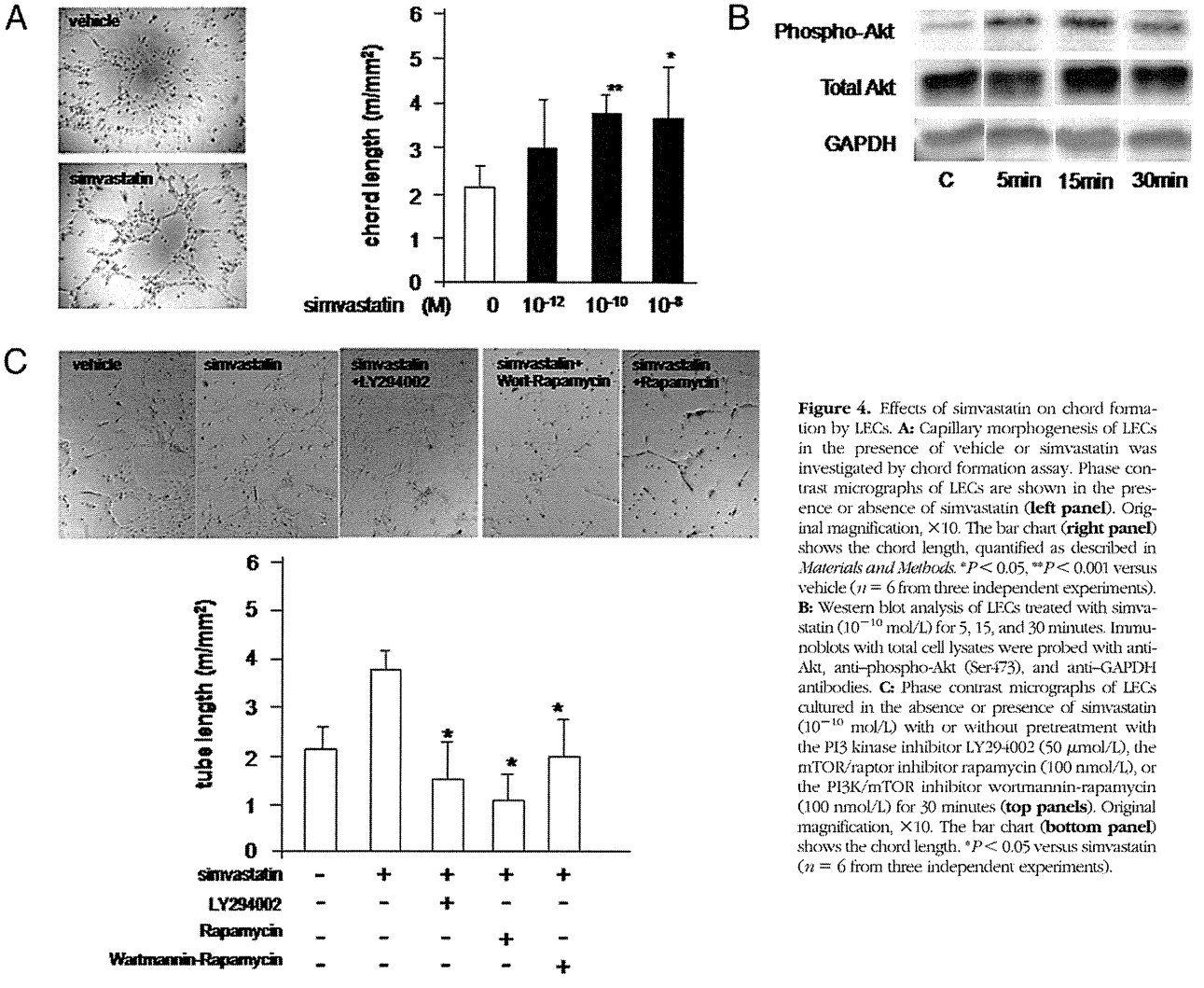

Figure 4. Effects of simvastatin on chord formation by LECs. **A:** Capillary morphogenesis of LECs in the presence of vehicle or simvastatin was investigated by chord formation assay. Phase contrast micrographs of LECs are shown in the presence or absence of simvastatin (**left panel**). Original magnification, ×10. The bar chart (**right panel**) shows the chord length, quantified as described in *Materials and Methods*. $^{*}P < 0.05$, $^{**}P < 0.001$ versus vehicle ($n = 6$ from three independent experiments). **B:** Western blot analysis of LECs treated with simvastatin (10^{-10} mol/L) for 5, 15, and 30 minutes. Immunoblots with total cell lysates were probed with anti-Akt, anti–phospho-Akt (Ser-473), and anti-GAPDH antibodies. **C:** Phase contrast micrographs of LECs cultured in the absence or presence of simvastatin (10^{-10} mol/L) with or without pretreatment with the PI3 kinase inhibitor LY294002 (50 μmol/L), the mTOR/raptor inhibitor rapamycin (100 nmol/L), or the PI3K/mTOR inhibitor wortmannin-rapamycin (100 nmol/L) for 30 minutes (**top panels**). Original magnification, ×10. The bar chart (**bottom panel**) shows the chord length. $^{*}P < 0.05$ versus simvastatin ($n = 6$ from three independent experiments).

simvastatin group. Simvastatin significantly enhanced wound vascularity based on image analysis of the percentage of the fluorescent area (9.29% ± 1.29% versus 3.25% ± 1.33%; $P < 0.001$)(Figure 2B). Wound lymphangiogenesis was analyzed by immunostaining of a LEC-specific marker, LYVE-1, in 10-μm frozen sections. Figure 3A shows new lymphatic vessels at the margin of simvastatin- or vehicle-treated wounds in diabetic mice on day 14. Wound lymphatic vascularity was significantly enhanced by simvastatin (percentage of fluorescent area: 1.72% ± 0.460% versus 0.395% ± 0.260%; $P < 0.001$) (Figure 3B). New vessels and lymphatics in granulation tissue in both groups were not covered with α-smooth muscle actin–positive mural cells (see Supplemental Figure S1 at *http://ajp.amjpathol.org*).

Simvastatin Induces Capillary Morphogenesis of LECs and Has an Antiapoptotic Effect but Does Not Induce Proliferation

To characterize the effects of simvastatin on lymphangiogenesis, we performed a chord formation assay in primary human LECs *in vitro*. Treatment with simvastatin promoted LEC chord formation in a dose-dependent manner (Figure 4A). This effect was significantly blocked by the PI3 kinase inhibitor LY294002, the mTOR inhibitor rapamycin, and the PI3/mTOR inhibitor wortmannin-rapamycin ($P < 0.05$)(Figure 4C). The proliferative and antiapoptotic effects of simvastatin on LECs were also examined because these are major effects of simvastatin in vascular endothelial cells. Simvastatin did not promote LEC proliferation, even at higher concentrations, and seemed to be slightly cytotoxic at 10^{-6} mol/L and 10^{-5} mol/L (Figure 5A). However, simvastatin treatment resulted in significant inhibition of H_2O_2-induced apoptosis compared with controls (Figure 5B).

Simvastatin Promotes Macrophage Infiltration and VEGF-C Production in Wounds

The number of macrophages in granulation tissues was evaluated in wounds on day 7. This timing was chosen because reepithelialization was almost complete on day 14 in simvastatin-treated wounds, and inflammatory cells had already diminished. The number of macrophages in simvastatin-treated wounds on day 7 was significantly

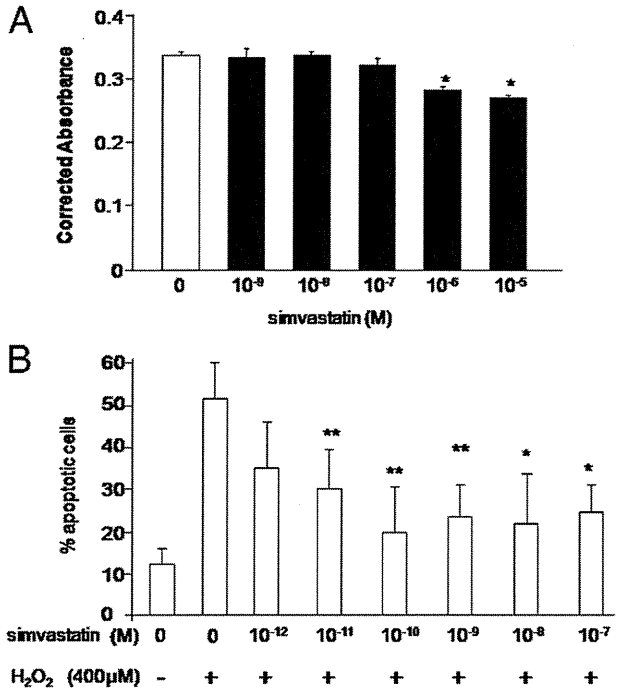

Figure 5. Effects of simvastatin on proliferation and apoptosis of LECs. **A:** Cell proliferation of LECs was investigated by MTS assay. Subconfluent cells (5000 cells per well) were reseeded on 96-well, flat-bottomed plates with 100 μL of growth media. The cells were treated with simvastatin and incubated for 48 hours at 37°C. Absorbance at 570 nm was recorded using a 96-well ELSIA plate reader. Quantification was performed as described in *Materials and Methods*. $^*P < 0.05$ versus vehicle ($n = 8$ from three independent experiments). **B:** Cell apoptosis in LECs was investigated by TUNEL assay. LECs were plated on chamber slides and placed in medium. Cells were stimulated by simvastatin and incubated for 24 hours with medium containing 400 μmol/L H_2O_2. Quantification of apoptotic cells was performed as described in *Materials and Methods*. $^*P < 0.05$, $^{**}P < 0.01$ versus H_2O_2 treatment ($n = 3$ from three independent experiments).

greater than that in controls (Figure 6, A and B). Most of the macrophages in the simvastatin-treated group expressed the M2 marker, IL-13, rather than the M1 marker, TNF-α, whereas most macrophages in the vehicle-treated group expressed TNF-α rather than IL-13 (Figure 6, C–F). The macrophages in the simvastatin-treated group produced VEGF-C (Figure 7A), and VEGF-C expression was significantly up-regulated in simvastatin-treated wounds compared with controls (Figure 7B). Other proangiogenic mediators in wound granulation tissue were evaluated by real-time PCR. Platelet-derived growth factor β, endothelial nitric oxide synthase, and fibroblast growth factor 2 were significantly up-regulated by simvastatin stimulation (see Supplemental Figure S2 at *http://ajp.amjpathol.org*).

Discussion

In this study, we found that topical application of simvastatin accelerated diabetic wound healing via promotion of angiogenesis and lymphangiogenesis. Many studies have reported that statins, including simvastatin, have strong angiogenic effects on vascular endothelial cells or placental stem cells and that these effects are mainly mediated by the PI3-kinase/Akt pathway,[11,22,23] although we note that other findings have also been reported[24] Consistent with these reports, abundant neovascularization and proangiogenic growth factors were observed in wounds treated with topical simvastatin in our *in vivo* study. Statins were originally introduced as systemic antihyperlipidemic drugs; however, a recent study has shown the value of topical simvastatin.[14] An advantage of topical application is that a suitable concentration of simvastatin can be applied without a risk of serious systemic adverse effects, such as rhabdomyolysis. Our results suggest that topical application of simvastatin could be a

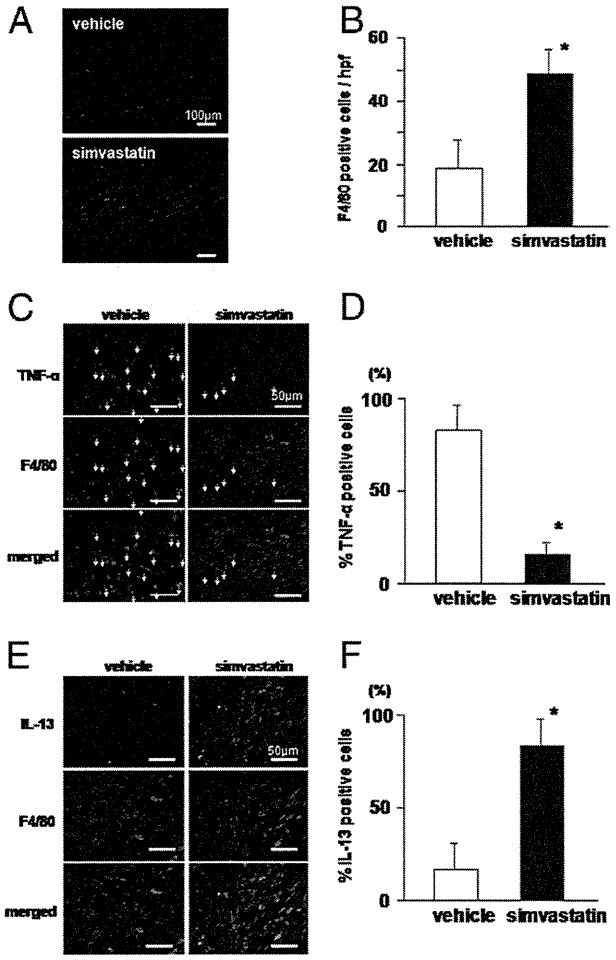

Figure 6. Effects of simvastatin on macrophage infiltration and phenotype in granulation tissue. **A:** Representative photomicrographs of the immunostained wound edge at 7 days after wound creation. Red fluorescence corresponds to F4/80-positive macrophages. Scale bar = 100 μm. **B:** The macrophage count, quantified as described in *Materials and Methods*. $^*P < 0.05$ versus vehicle ($n = 5$). **C:** Representative photomicrographs of the immunodetection of TNF-α and F4/80 in histologic sections from vehicle- or simvastatin-treated wounds (original magnification ×400). Scale bar = 50 μm. Green and red fluorescence corresponds to TNF-α–positive cells and F4/80-positive macrophages, respectively. Yellow indicates TNF-α–producing M1 phenotype macrophages (**white arrows**). **D:** Quantification of percentage of TNF-α–positive macrophages, as described in *Materials and Methods*. $^*P < 0.001$ versus vehicle ($n = 5$ in each group). **E:** Representative photomicrographs of immunodetection of IL-13 and F4/80 in histologic sections from vehicle- or simvastatin-treated wounds (original magnification ×400). Scale bar = 50 μm. Green and red fluorescence correspond to IL-13–positive cells and F4/80-positive macrophages, respectively. Yellow indicates IL-13–producing M2 phenotype macrophages. **F:** Quantification of percentage of IL-13–positive macrophages, as described in *Materials and Methods*. $^*P < 0.001$ versus vehicle ($n = 5$ in each group).